

1 **Replies to AE**

2 Dear authors,

3 both the Referees acknowledge a significant improvement of the manuscript, but the two
4 judgements are split. Regarding the issues, raised by the second Referee, about the results scarcely
5 supported by the (few) data about soil moisture, I see his point (squeezing too much the data to get
6 results), especially considering that the same data set has been already used in other papers of your
7 group, as highlighted by Referee #1 (one of them is currently under consideration for possible
8 publication in HESS).

9 So, to try to make this manuscript acceptable for publication in HESS, I invite to do as much as
10 you can to demonstrate that the results you present, although poorly significant for the case under
11 study, may represent an example of a possible methodology to improve currently adopted
12 approaches to landslide hazard assessment. Also the other major concern by Referee #2, about the
13 validation of the results, should be carefully considered in revising the manuscript, as well as other
14 comments which were not addressed and to which a convincing rebuttal was not provided during
15 the first round of review.

16 I look forward to receiving a newly revised version.

17 Best regards,

18 Roberto Greco

19 Reply: We thank the AE and reviewer's comments on further improving the manuscript.
20 Regarding using the 'same datasets' for the other papers in our group, it is important to clarify that
21 although the 3 papers use the same landslide event records, they all use different landslide
22 triggering data/methods. This paper uses the WRF derived multi-layer soil moisture information
23 to work out the landslide initiation threshold, which is the first attempt of its kind which has not
24 been done by previous studies. Such a dataset is globally available with high spatial and temporal
25 resolution, so it has the advantage over satellite (as compared in the last updated manuscript with
26 our previous J-STARS paper) and rain gauge networks (as discussed in Introduction). We have
27 added this clarification in the revised manuscript.

28 In addition, we have explored the spatial variation of soil moisture to demonstrate the soil moisture
29 representation of a single soil moisture sensor over a large region (these new results are added in
30 the latest version of the manuscript). Again, this is a novel approach in the landslide study. Based
31 on the newly added results, although there is a significant elevation difference in the region, a
32 single soil moisture sensor has high representation of a significant proportion of the study area as
33 demonstrated by the correlation analysis. Although there is still a small proportion of the areas
34 where the correlation is poor, this has prompt us to carry out a future study on the optimal design
35 of soil moisture sensor network for landslide study. The need for such a study is based on the fact
36 that there has been a lot of studies on the optimal rain gauge network design, but similar research
37 on soil moisture sensor network design has been largely ignored by the research community. The
38 WRF derived soil moisture data has a potential to provide the important soil moisture spatial
39 information for an optimal design of soil moisture sensor network, which will be carried out via

40 Principal Component Analysis and cluster analysis. Therefore, the study described in the current
41 paper has paved a foundation for such a research.

42 We admit that this paper clearly cannot solve all the problems, but the results and methods are new
43 which deserve to be known by the community. We have attached the updated manuscript for your
44 consideration.

45 Yours Sincerely

46 Lu Zhuo, the lead author

47

48

49

Replies to Reviewer 2

MAJOR FLAWS

51 1- The use of a single measuring station located in a completely different setting is still an
52 open issue in my opinion. The authors provided some justification (only available station)
53 and heavily modified the evaluation section. This is not enough. In my opinion a
54 publication in an important journal like HESS demands good data and good results. I
55 appreciated the methodology developed in your paper but you just do not have good
56 amount and quality of data, therefore you are borderline. You cannot use an excuse that
57 these are the best data you could get in this test site: limited data prevent to get reliable and
58 robust outcomes, thus endangering publication. In my first report (general issue #4), I
59 suggested an approach to overcome this situation, but you didn't implement it in the revised
60 manuscript. I briefly outline it again (this is just a quick sum-up, please develop it further
61 and add these concepts in different places in the manuscript, where appropriate). One
62 measuring station in the whole area is not sufficient to adequately calibrate the model (this
63 must be stated clearly) and can be used only to build a methodology and to obtain only
64 preliminary results. However, from this preliminary steps, relevant outcomes could be
65 obtained: other studies in the same test site established empirical correlations between
66 landslides and hydrogeological variables on smaller territorial units (see details in my
67 previous general issue #4). Thus, it could be inferred that the proposed methodology is
68 preliminary but it could be further refined (and better result could be obtained) if data from
69 a denser measuring network would be available.

70 2- Validation. What I understand from the latest version of your paper is the following: You
71 model soil moisture and rainfall. You provide a spatial validation only for the modeled
72 rainfall. You use the soil moisture modeled across the whole region. I think this is not
73 correct. This issue is related to the previous one: a measuring station in the alluvial plain
74 cannot be used to calibrate a soil moisture model in mountains hundreds of kilometers
75 away. However, you did it, you got some results in trying to predict landslides, you need
76 to add that more measuring instruments would allow for a better calibration potentially
77 improving the overall results.

78 Reply:

79 We thank the reviewer for raising the soil moisture sensor representation problem. We have
80 added the following clarifications in the updated manuscript:

81 -----

82 For the WRF soil moisture evaluation, clearly the evaluation work based on a single soil
83 moisture sensor located in plain area is not sufficient to derive conclusions about the model's
84 performance over the whole study region. Therefore, the results are preliminary here. However,
85 in this study, by introducing the WRF spatial soil moisture information into the landslide
86 prediction model, the performance indeed has been improved in comparison with our previous
87 study using the satellite remote sensing soil moisture data (Zhuo et. al 2019). A similar concept
88 has been carried out by Segoni et al., (2018b), who implemented the soil moisture information
89 simulated from a hydrological model into a regional landslide early warning system with clear
90 improvements in false/ missing alarm performance. Although the results shown in this study
91 is preliminary and confined by the study area, the improved landslide prediction performance
92 is already obtained. Therefore, it is hoped with more densely soil moisture network data
93 available globally and further refinements of the method, the results could be improved further.

94 -----

95 In addition, ideally, it will be useful if there is a dense in-situ soil moisture sensing network
96 covering the whole study area. In reality, that's not practical, so we have to rely on the spatial soil
97 moisture information by other means. So far, the soil moisture data with the best spatial and
98 temporal resolution is from the WRF model. A question is about how representative of a single
99 soil moisture sensor for the whole study area. We have carried out the correlation study of the
100 single sensor with the whole study region (added in the discussion section). The initial assumption
101 is that the soil moisture sensor can only represent its adjacent area, but the result was a surprise.
102 Based on the results, a single point can represent a significant proportion of the region. Admittedly,
103 there are some areas where the correlations are poor and further studies are needed to find out why
104 some areas are highly correlated whereas others are not. This has prompt us to do a future study
105 on the optimal soil moisture sensor network design for landside applications. Although there are
106 numerous studies on the rain gauge network design by the research community, the soil moisture
107 sensor network design has been largely ignored by the community. Therefore, this study has paved
108 a foundation for such research.

109 ---

110
111 **PREVIOUS COMMENTS NOT ADDRESSED**

112 - Former general issue #4: see also my general comment. You "dodged" the problem by
113 validating rainfall instead of soil moisture. But in the manuscript you use soil moisture,
114 therefore the problem remains still open.

115 Reply: Please see the reply above.

116 - Former specific issue L40-42. I can't find any trace of this. Maybe because you deleted
117 relevant parts of the introduction?

118 Reply: We thank the reviewer for providing us with the detailed references on the rainfall
119 landslide prediction methods. Since this study is focused on the soil moisture landslide
120 application, after reading the introduction section several times, we decided to remove this part
121 to avoid potential confusion.

122 - Former specific issue Line 628. I suggested to check line 628, not to check the references.
123 Sorry for the misunderstanding (I wrote last comment and the reference list too close each
124 other).

125 Reply: The former specific issue Line 628 was not supposed to be there, which is now removed.

126 ---

127 128 GENERAL COMMENTS

129 The validation of the rainfall does not seem to provide good results: a R value of 0.40 seems
130 rather low to me. You make reference to another work in the USA that gets similar values, but
131 I think that the standards in the international literature are higher than this.
132 Results, discussion and conclusion are not well separated. The results section includes some
133 interpretation of the results (usually more convenient in the discussion). If the
134 discussion/conclusion section becomes too long, maybe it would be better to split discussion
135 and conclusions.

136 Reply: We agree that the rainfall validation is not good in this case study. Rainfall is one of
137 the main drivers of soil moisture change, and it is logical to think soil moisture and rainfall are
138 highly linked. However, because rainfall temporal variation is of high frequency while soil
139 moisture is of low frequency, they behave differently. The results illustrate that for landslide
140 study, it is better to use the WRF soil moisture data rather than its rainfall data. Clearly more
141 studies are needed to confirm this assumption. We have included this explanation in the
142 updated manuscript.

143 We agree with the reviewer that some of the interpretation parts in the result section should be
144 moved to the discussion section. Since we have further added some new results in the
145 discussion section. We have split the discussion and conclusion into two separate parts.

146 ---

147 148 MINOR COMMENTS

149 Please, check the bi-directional correspondence between the references in the text and in the
150 reference list, as you have modified the introduction and it seems to me that some discrepancies
151 exist (e.g. Zhuo et al 2016 is cited at line 80 but it is not in the reference list).

152 Reply: The discrepancies are caused by the Endnote reference software, which occurred in the
153 'tracked changes' version only (e.g., Zhuo et al 2016 has been removed in the 'updated'
154 version). In this submission, we will make sure the discrepancies dont happen again.

155 L78. The new added sentence needs some reference.

156 Reply: The relevant references have been added in the updated manuscript.

157 In the first part of section 4.1 (e.g. L365 or 366), please clarify that the comparison is carried
158 out at a single point: the one where the measuring station is located.

159 Reply: This has been clarified throughout the updated manuscript. "In this study, we carry out
160 a temporal comparison between all the three WRF soil moisture products with the in-situ
161 observations (at a single soil moisture measuring point in the plain area)"

162 L441. Which works? Please be more specific.

163 Reply: It refers to the works mentioned in the introduction section. We have specified this in
164 the updated manuscript, but the references are not repeated in this section. "As introduced at
165 the beginning of the paper, previous works (as discussed in the Introduction) have
166 demonstrated that in complex geomorphologic settings (e.g., in Emilia Romagna), a rainfall
167 threshold approach is too simple and more hydrologically driven approaches need to be
168 established."

169 L465-466. I don't agree with this reason. You are dealing with landslides, not with pure
170 statistics, therefore the statistical reliability of this approach is questionable. I think it is better
171 to state in the premises that your objective is to have equal coverage areas, consequently you
172 identified those class-break values.

173 Reply: As suggested by the reviewer, the sentence has been updated as "There are different
174 ways to group the slopes. In this study, in order to have equal coverage areas, we have
175 identified these class-break values."

176 L519. Many shallow instead of very shallow?

177 Reply: We mean very shallow, but to avoid confusion, we have changed the sentence to "Third,
178 the landslides occurred in the region are mainly in the top shallow soil layer".

179 L549. Which study? Please provide a reference.

180 Reply: The relevant reference has been added. "The WRF rainfall performance is found to be
181 similar to a study carried out over the central USA (Van Den Broeke et al., 2018)."

182 L560-568- I suggest deleting this whole part as it includes issues like civil protection
183 procedures, risk perception, risk management and it goes beyond the scopes of your work.

184 Reply: We agree. This part has been deleted.

185 L570 Which studies? Please provide references.

186 Reply: The relevant reference has been added. “Here, WRF is modelled based on the ERA-
187 Interim datasets, however, it has been found in Albergel et al. (2018), the performance of using
188 the ERA5 has surpassed the ERA-Interim.”

189 L580 Here some reference are needed. I suggest using Nichol and Wong 2005 for remote
190 sensing (feel free to add more examples). In addition, I suggest to add also the possibility to
191 use internet news to detect all relevant landslides (all landslides with a relevant impact on
192 society will be reported on internet news), also using automatic methods (Battistini et al.,
193 2013).

194 Reply: The suggested contents have been added. “Other ways of expanding the current
195 landslide catalog can depend on automatic landslide detection methods based on remote
196 sensing images (Nichol and Wong, 2005;Chen et al., 2018), internet news (as all landslides
197 with a relevant impact on society will be reported on internet news), and automatic web data
198 mining methods (Battistini et al., 2013;Goswami et al., 2018)”

199 L588. I would add: “However, the methodology could be replicated to derive site-specific
200 calibrations of the approach proposed.”

201 Reply: This has been changed to “One must bear in mind that although the results demonstrated
202 in this study are only valid for the selected region, the methodology could be generalised to
203 derive site-specific calibrations in other sites using the proposed approach.”

204 ---

205 REFERENCES CITED:

- 206 Battistini, A., Segoni, S., Manzo, G., Catani, F., & Casagli, N. (2013). Web data mining for
207 automatic inventory of geohazards at national scale. *Applied Geography*, 43, 147-158.
208 Nichol, J., & Wong, M. S. (2005). Satellite remote sensing for detailed landslide inventories using
209 change detection and image fusion. *International journal of remote sensing*, 26(9), 1913-1926.

210

Assessment of Simulated Soil Moisture from WRF Noah, Noah-MP, and CLM Land Surface Schemes for Landslide Hazard Application

Lu Zhuo¹, Qiang Dai^{1,2*}, Dawei Han¹, Ningsheng Chen³, Binru Zhao^{1,4}

¹WEMRC, Department of Civil Engineering, University of Bristol, Bristol, UK

²Key Laboratory of VGE of Ministry of Education, Nanjing Normal University, Nanjing, China

³The Institute of Mountain Hazards and Environment (IMHE), China

⁴College of Water Conservancy and Hydropower Engineering, Hohai University, Nanjing, China

*Correspondence: civengwater@gmail.com

Abstract

This study assesses the usability of Weather Research and Forecasting (WRF) model simulated soil moisture for landslide monitoring in the Emilia Romagna region, northern Italy during the 10-year period between 2006 and 2015. Particularly three advanced Land Surface Model (LSM) schemes (i.e., Noah, Noah-MP and CLM4) integrated with the WRF are used to provide detailed multi-layer soil moisture information. Through the temporal evaluation with the single-point in-situ soil moisture observations, Noah-MP is the only scheme that is able to simulate the large soil drying phenomenon close to the observations during the dry season, and it also has the highest correlation coefficient and the lowest *RMSE* at most soil layers. **It is also demonstrated that a single soil moisture sensor located in plain area has high correlation with a significant proportion of the study area (even in the mountainous region 141 km away, based on the WRF simulated spatial soil moisture information).** The evaluation of the WRF rainfall estimation shows there is no distinct difference among the three LSMs, and their performances are in line with a published study for the central USA. Each simulated soil moisture product from the three LSM schemes is then used to build a landslide prediction model, and within each model, 17 different exceedance probability levels from 1% to 50% are adopted to determine the optimal threshold scenario (in total there are 612 scenarios). Slope degree information is also used to separate the study region into different

236 groups. The threshold evaluation performance is based on the landslide forecasting accuracy using
237 45 selected rainfall events between 2014-2015. Contingency tables, statistical indicators, and
238 Receiver Operating Characteristic analysis for different threshold scenarios are explored. The
239 results have shown that, for landslide monitoring, Noah-MP at the surface soil layer with 30%
240 exceedance probability provides the best landslide monitoring performance, with its hitting rate at
241 0.769, and its false alarm rate at 0.289.

242 **Keywords:** Emilia Romagna, Weather Research and Forecasting (WRF) Model, Land Surface
243 Model (LSM), Numerical Weather Prediction (NWP) model, landslide hazards, soil moisture.

244 1. Introduction

245 Landslide is a repeated geological hazard during rainfall seasons, which causes massive
246 destructions, loss of lives, and economic damages worldwide (Klose et al., 2014). The accurate
247 predicting and monitoring of the spatiotemporal occurrence of the landslide is the key to prevent/
248 reduce casualties and damages to properties and infrastructures. One of the most widely adopted
249 methods for landslide prediction is based on rainfall threshold, which relies on building the rainfall
250 intensity-duration curve using the information from the past landslide events (Chae et al., 2017).
251 However, such a method in many cases is insufficient for landslide hazard assessment (Posner and
252 Georgakakos, 2015), because in addition to rainfall, initial soil moisture condition is one of the
253 main triggering factors of the events (Glade et al., 2000; Crozier, 1999; Tsai and Chen, 2010; Hawke
254 and McConchie, 2011; Bittelli et al., 2012; Segoni et al., 2018b; Valenzuela et al., 2018; Bogaard
255 and Greco, 2018).

256 For landslide applications, one potential soil moisture estimation method is through satellite
257 remote sensing technologies. Although such technologies have been improved significantly over

258 the past decade, their retrieving accuracy is still largely affected by frozen soil conditions (Zhuo
259 et al., 2015a), and dense vegetation coverages particularly in mountainous regions (Temimi et al.,
260 2010); furthermore, the acquired data only covers the top few centimetres of soil. Although the
261 more recently launched satellites such as Sentinel-1 (1 km, and 3 days resolution) has shown some
262 promising performance of soil moisture estimation (Gao et al., 2017;Paloscia et al., 2013), its
263 availability only covers the recent years (Geudtner et al., 2014). Those disadvantages restrict the
264 full utilisation of satellite soil moisture products for landslide monitoring application as discussed
265 in our previous study (Zhuo et al., 2019). In Zhuo et al. (2019), it is discussed that both the temporal
266 and spatial resolutions of the ESA CCI satellite soil moisture product (Dorigo et al., 2017) is too
267 coarse for landslide applications, and its data are mostly only available after the year 2002.
268 Moreover, the shallow depth soil moisture observation from the satellite hinders the accuracy of
269 landslide predictions. Therefore, other alternative soil moisture estimation methods need to be
270 explored.

271 One emerging area relies on modelling. Some studies have used modelled soil moisture data for
272 landslide applications (Ponziani et al., 2012;Ciabatta et al., 2016;Zhao et al., 2019a;Zhao et al.,
273 2019b). However, to our knowledge, there is a lack of existing study using the state-of-the-art
274 Land Surface Models (LSMs) modelled soil moisture for landslide studies, such as the Noah LSM
275 (Ek et al., 2003) and the Community Land Model (CLM) (Oleson et al., 2010). LSMs describe the
276 interactions between the atmosphere and the land surface by simulating exchanges of momentum,
277 heat and water within the Earth system (Maheu et al., 2018). They are capable of simulating the
278 most important subsurface hydrological processes (e.g., soil moisture) and can be integrated with
279 the advanced Numerical Weather Prediction (NWP) system like WRF (Weather Research and
280 Forecasting) (Skamarock et al., 2008) for comprehensive soil moisture estimations (i.e., through

281 the surface energy balance, the surface layer stability and the water balance equations) (Greve et
282 al., 2013). NWP-based (i.e., with integrated LSM, thereafter) soil moisture estimations have many
283 advantages, for instance their spatial and temporal resolution can be set at different scales
284 depending on the input datasets to fit various application requirements; their coverage is global,
285 and the estimated soil moisture data covers multiple soil layers (from the shallow surface layer to
286 deep root-zones); as well as a number of globally-covered data products can provide the necessary
287 boundary and initial conditions for running the models. Soil moisture estimated through such an
288 approach has been widely recognised and demonstrated in many studies, which cover a broad
289 range of applications from hydrological modelling (Srivastava et al., 2013a;Srivastava et al., 2015),
290 drought studies (Zaitchik et al., 2013), flood investigations (Leung and Qian, 2009), to regional
291 weather prediction (Stéfanon et al., 2014). Therefore, NWP-based soil moisture datasets could
292 provide valuable information for landslide applications. However, to our knowledge, relevant
293 research has never been carried out.

294 The aim of this study hence is to evaluate the usefulness of NWP modelled soil moisture for
295 landslide monitoring. Here the advanced WRF model (version 3.8) is adopted, because it offers
296 numerous physics options such as micro-physics, surface physics, atmospheric radiation physics,
297 and planetary boundary layer physics (Srivastava et al., 2015), and can integrate with a number of
298 LSM schemes, each varying in physical parameterisation complexities. So far there is limited
299 literature in comparing the soil moisture accuracy of different LSMs options in the WRF model.
300 Therefore, in this study, we select three of the WRF's most advanced LSM schemes (i.e., Noah,
301 Noah-Multiparameterization (Noah-MP), and CLM4) to compare their soil moisture performance
302 for landslide hazard assessment. Furthermore, since all the three schemes can provide multi-layer
303 soil moisture information, it is useful to include all those simulations for the comparison so that

304 the optimal depth of soil moisture could be determined for the landslide monitoring application.
305 In order to compare with the performance of our previous study on using the satellite soil moisture
306 data (Zhuo et al., 2019), the same study area called Emilia Romagna is used here. The study period
307 covers 10 years from 2006 to 2015 to include a long-term record of landslide events. In addition,
308 because slope angle is one of the major factors controlling the stability of the slope, it is hence
309 used in this study to divide the study area into several slope groups, so that a more accurate
310 landslide prediction model could be built.

311 The description of the study area and the used datasets are included in Section 2. Methodologies
312 regarding the WRF model, the related LSM schemes and the adopted landslide threshold
313 evaluation approach are provided in Section 3. Section 4 shows the WRF soil moisture evaluation
314 results against the in-situ observations, and the WRF rainfall evaluations over the whole study area.
315 Section 5 covers the comparison results of the WRF modelled soil moisture products for landslide
316 applications. The discussions and conclusions of the study are included in Section 6 **and 7**
317 **respectively**.

318 **2. Study Area and Datasets**

319 **2.1 Study Area**

320 The study area is in the Emilia Romagna Region, northern Italy (Figure 1). Its population density
321 is high. The region has high mountainous areas in the S-SW, and wide plain areas towards NE,
322 with a large elevation difference (i.e., 0 m to 2125 m) across 50 km distance from the north to the
323 south (Rossi et al., 2010). The region has a mild Mediterranean climate with distinct wet and dry
324 seasons (i.e., dry season between May and October, and wet season between November and April).
325 The study area tends to be affected by landslide events easily, with approximately one-fifth of the

326 mountainous zone covered by active or dormant landslide deposits (Bertolini et al., 2005). Rainfall
327 is by far the primary triggering factor of landslides in the region, followed by snow melting:
328 shallow landslides are mainly triggered by short but exceptionally intense rainfall, and long and
329 moderate rainfall events over saturated conditions, while deep-seated landslides have a more
330 complex response to rainfall and are mainly caused by moderate but exceptionally prolonged (even
331 up to 6 months) periods of rainfalls (Segoni et al., 2015). Due to the abundant data available in the
332 region, several studies on regional scale landslide prediction and early warning have been
333 published (Berti et al., 2012;Martelloni et al., 2012;Lagomarsino et al., 2015;Segoni et al.,
334 2018b;Segoni et al., 2018a;Lagomarsino et al., 2013). Interested readers can refer to those studies
335 for more information.

336 **2.2 Selection of The Landslide Events**

337 The landslides catalog is collected from the Emilia Romagna Geological Survey (Berti et al., 2012).
338 The information included in the catalog are: location, date of occurrence, the uncertainty of date,
339 landslide characteristics (dimensions, type, and material), triggering factors, damages, casualties,
340 and references. Unfortunately, many pieces of the information are missing from the records in
341 many cases. In order to organise the data in a more systematic way so that only the relevant events
342 are retained, a two-step event selection procedure is initially carried out based on: 1) rainfall-
343 induced only; and 2) high spatial-temporal accuracy (exact date and coordinates). Finally, a
344 revision of the information about the type of slope instabilities such as landslide/debris
345 flow/rockfall and the characteristics of the affected slope (natural or artificial) is also carried out
346 over the selected records (Valenzuela et al., 2018). The catalog period used in this study covers
347 between 2006 and 2015, which is in accordance with the WRF model run. After filtering the data
348 records, only one-fifth of them (i.e., 157 events) is retained. The retained events are shown as

349 single circles in Figure 2, with slope information (calculated through the Digital Elevation Model
350 (DEM) data) also presented in the background. It can be seen the spatial distribution of the
351 occurred landslide events is very heterogeneous, with nearly all of them occurred in the hilly
352 regions.

353 **2.3 Datasets**

354 There is a total of 19 soil moisture stations available within the study area, however, based on our
355 collected data, only one of them at the San Pietro Capofiume (latitude 44° 39' 13.59", longitude
356 11° 37' 21.6") provides long-term valid soil moisture retrievals (i.e., 2006 to 2017). We have
357 checked the data from all the rest of the stations, they are either absent (or have very big data gaps)
358 or do not cover the research period at all. Therefore, only the San Pietro Capofiume station is used
359 for the WRF soil moisture temporal evaluation. The soil moisture is measured from 10 cm to 180
360 cm deep in the soil at 5 depths, by the Time Domain Reflectometry (TDR) instrument. Data are
361 recorded in the unit of volumetric water content (m^3/m^3) and at daily timestep (Pistocchi et al.,
362 2008). The data used in this study is between 2006 and 2015. Rainfall data over the whole study
363 area is collected from over 200 tipping-bucket rain gauges, which are used to assess the quality of
364 the WRF model's rainfall estimations in the study area, as well as for rainfall events selection
365 during the Year 2014 and 2015.

366 To drive a NWP model like WRF for soil moisture simulations, several globally-coved data
367 products can be chosen for extracting the boundary and initial conditions information, for instance,
368 the European Centre for Medium-Range Weather Forecasts (ECMWF) reanalysis (ERA-Interim)
369 and the National Centre for Environmental Prediction (NCEP) reanalysis are two of the most
370 commonly used data products. It has been found by (Srivastava et al., 2013b) that the ERA-Interim
371 datasets can provide better boundary conditions than the NCEP datasets for WRF hydro-

372 meteorological predictions in Europe, which is therefore adopted in this study to drive the WRF
373 model. The spatial resolution of the ERA-Interim is approximately 80 km. The data is available
374 from 1979 to present, containing 6-hourly gridded estimates of three-dimensional meteorological
375 variables, and 3-hourly estimates of a large number of surface parameters and other two-
376 dimensional fields. A comprehensive description of the ERA-Interim datasets can be found in (Dee
377 et al., 2011)

378 The Shuttle Radar Topography Mission (SRTM) 3 Arc-Second Global (~ 90m) DEM datasets are
379 downloaded and used as the basis for the slope degree calculations. SRTM DEM data has been
380 widely used for elevation-related studies worldwide due to its high quality, near-global coverage,
381 and free availability (Berry et al., 2007).

382 **3. Methodologies**

383 **3.1 WRF Model and The Three Land Surface Model Schemes**

384 The WRF model is a next-generation, non-hydrostatic mesoscale NWP system designed for both
385 atmospheric research and operational forecasting applications (Skamarock et al., 2005). The model
386 is powerful enough in modelling a broad range of meteorological applications varying from tens
387 of metres to thousands of kilometres (NCAR, 2018). It has two dynamical solvers: the ARW
388 (Advanced Research WRF) core and the NMM (Nonhydrostatic Mesoscale Model) core. The
389 former has more complex dynamic and physics settings than the latter which only has limited
390 setting choices. Hence in this study WRF with ARW dynamic core (version 3.8) is used to perform
391 all the soil moisture simulations.

392 The main task of LSM within the WRF is to integrate information generated through the surface
393 layer scheme, the radiative forcing from the radiation scheme, the precipitation forcing from the

394 microphysics and convective schemes, and the land surface conditions to simulate the water and
395 energy fluxes (Ek et al., 2003). WRF provides several LSM options, among which three of them
396 are selected in this study as mentioned in the introduction: Noah, Noah-MP, and CLM4. Table 1
397 gives a simple comparison of the three models. The detailed description of the models is written
398 below in the order of increasing complexity in regards of the way they deal with thermal and
399 moisture fluxes in various layers of soil, and their vegetation, root and canopy effects
400 (Skamarock et al., 2008).

401 **3.1.1 Noah**

402 Noah is the most basic amongst the three selected LSMs. It is one of the ‘second generation’ LSMs
403 that relies on both soil and vegetation processes for water budgets and surface energy closures
404 (Wei et al., 2010). The model is capable of modelling soil and land surface temperature, snow
405 water equivalent, as well as the general water and energy fluxes. The model includes four soil
406 layers that reach a total depth of 2 m in which soil moisture is calculated. Its bulk layer of canopy
407 -snow-soil (i.e., lack the abilities in simulating photosynthetically active radiation (PAR),
408 vegetation temperature, correlated energy, and water, heat and carbon fluxes), ‘leaky’ bottom (i.e.,
409 drained water is removed immediately from the bottom of the soil column which can result in
410 much fewer memories of antecedent weather and climate fluctuations) and simple snow melt-thaw
411 dynamics are seen as the model’s demerits (Wharton et al., 2013). Noah calculates the soil moisture
412 from the diffusive form of Richard’s equation for each of the soil layer (Greve et al., 2013), and
413 the evapotranspiration from the Ball-Berry equation (considering both the water flow mechanism
414 within soil column and vegetation, as well as the physiology of photosynthesis (Wharton et al.,
415 2013)).

416 **3.1.2 Noah-MP**

417 Noah-MP (Niu et al., 2011) is an improved version of the Noah LSM, in the aspect of better
418 representations of terrestrial biophysical and hydrological processes. Major physical mechanism
419 improvements directly relevant to soil water simulations include: 1) introducing a more permeable
420 frozen soil by separating permeable and impermeable fractions (Cai, 2015), 2) adding an
421 unconfined aquifer immediately beneath the bottom of the soil column to allow the exchange of
422 water between them (Liang et al., 2003), and 3) the adoption of a TOPMODEL (TOPography
423 based hydrological MODEL)-based runoff scheme (Niu et al., 2005) and a simple SIMGM
424 groundwater model (Niu et al., 2007) which are both important in improving the modelling of soil
425 hydrology. Noah-MP is unique compared with the other LSMs, as it is capable of generating
426 thousands of parameterisation schemes through the different combinations of “dynamic leaf,
427 canopy stomatal resistance, runoff and groundwater, a soil moisture factor controlling stomatal
428 resistance (the β factor), and six other processes” (Cai, 2015). The scheme option used in the study
429 are: Ball-Berry scheme for canopy stomatal resistance, Monin-Obukhov scheme for surface layer
430 drag coefficient calculation, the Noah based soil moisture factor for stomatal resistance, the
431 TOPMODEL runoff with the SIMGM groundwater, the linear effect scheme for soil permeability,
432 the two-stream applied to vegetated fraction scheme for radiative transfer, the CLASS (Canadian
433 Land Surface Scheme) scheme for ground surface albedo option, and the Jordan (Jordan, 1991)
434 scheme for partitioning precipitation between snow and rain.

435 **3.1.3. CLM4**

436 CLM4 is developed by the National Center for Atmospheric Research (NCAR) to serve as the land
437 component of its Community Earth System Model (formerly known as the Community Climate
438 System Model) (Lawrence et al., 2012). It is a ‘third generation’ model that incorporates the
439 interactions of both nitrogen and carbon in the calculations of water and energy fluxes. Compared

440 with its previous versions, CLM4 (Oleson et al., 2008) has multiple enhancements relevant to soil
441 moisture computing. For instance, the model's soil moisture is estimated by adopting an improved
442 one-dimensional Richards equation (Zeng and Decker, 2009); the new version allows the dynamic
443 interchanges of soil water and groundwater through an improved definition of the soil column's
444 lower boundary condition that is similar to the Noah-MP's (Niu et al., 2007). Furthermore, the
445 thermal and hydrologic properties of organic soil are included for the modelling which is based on
446 the method developed in (Lawrence and Slater, 2008). The total ground column is extended to 42
447 m depth, consisting 10 soil layers unevenly spaced between the top layer (0.0–1.8 cm) and the
448 bottom layers (229.6–380.2 cm), and 5 bedrock layers to the bottom of the ground column
449 (Lawrence et al., 2011). Soil moisture is estimated for each soil layer.

450 **3.2 WRF Model Parameterization**

451 The WRF model is centred over the Emilia Romagna Region with three nested domains (D1, D2,
452 D3 with the horizontal grid sizes of 45 km, 15 km, and 5 km, respectively), of which the innermost
453 domain (D3, with 88 x 52 grids (west-east and south-north, respectively)) is used in this study. A
454 two-way nesting scheme is adopted allowing information from the child domain to be fed back to
455 the parent domain. With atmospheric forcing, static inputs (e.g., soil and vegetation types), and
456 parameters, the WRF model needs to be spin-up to reach its equilibrium state before it can be used
457 (Cai et al., 2014;Cai, 2015). In this study, WRF is spin-up by running through the whole year of
458 2005. After the spin-up, the WRF model for each of the selected LSM scheme is executed in daily
459 timestep from January 1, 2006, to December 31, 2015, using the ERA-Interim datasets.

460 The microphysics scheme plays a vital role in simulating accurate rainfall information which in
461 turn is important for modelling the accurate soil moisture variations. WRF V3.8 is supporting 23
462 microphysics options range from simple to more sophisticated mixed-phase physical options. In

463 this study, the WRF Single-Moment 6-class scheme is adopted which considers ice, snow and
464 graupel processes and is suitable for high-resolution applications (Zaidi and Gisen, 2018). The
465 physical options used in the WRF setup are Dudhia shortwave radiation (Dudhia, 1989) and Rapid
466 Radiative Transfer Model (RRTM) longwave radiation (Mlawer et al., 1997). Cumulus
467 parameterization is based on the Kain-Fritsch scheme (Kain, 2004) which is capable of
468 representing sub-grid scale features of the updraft and rain processes, and such a capability is
469 beneficial for real-time modelling (Gilliland and Rowe, 2007). The surface layer parameterization
470 is based on the Revised fifth-generation Pennsylvania State University–National Center for
471 Atmospheric Research Mesoscale Model (MM5) Monin-Obukhov scheme (Jiménez et al., 2012).
472 The Yonsei University scheme (Hong et al., 2006) is selected to calculate the planetary boundary
473 layer. The parameterization schemes used in the WRF modelling are shown in Table 2. The
474 datasets for land use and soil texture are available in the pre-processing package of WRF. In this
475 study, the land use categorisation is interpolated from the MODIS 21-category data classified by
476 the International Geosphere Biosphere Programme (IGBP). The soil texture data are based on the
477 Food and Agriculture Organization of the United Nations Global 5-minutes soil database.

478 **3.3 Translation of Observed and Simulated Soil Moisture Data to Common Soil Layers**

479 Since all soil moisture datasets have different soil depths, it is difficult for a direct comparison.
480 The Noah and Noah-MP models include four soil layers, centred at 5, 25, 70, and 150 cm,
481 respectively. Whereas CLM4 model has 10 soil layers, centered at 0.9, 3.2, 6.85, 12.85, 22.8, 39.2,
482 66.2, 110.65, 183.95, 304.9 cm, respectively. Moreover, the in-situ sensor measures soil moisture
483 centred at 10, 25, 70, 135, and 180 cm. In order to make the datasets comparable at consistent soil
484 depths, the simple linear interpolation approach described in (Zhuo et al., 2015b) is applied in this
485 study, and a benchmark of the soil layer centred at 10, 25, 70 and 150 cm is adopted.

486 3.4 Soil Moisture Thresholds Build Up and Evaluations

487 To build and evaluate the soil moisture thresholds for landslides forecasting, all datasets have been
488 grouped into two portions: 2006-2013 for the establishment of thresholds, and 2014-2015 for the
489 evaluation. The determination of soil moisture thresholds is based on determining the most suitable
490 soil moisture triggering level for landslides occurrence by trying a range of exceedance
491 probabilities (percentiles). For example, a 10% exceedance probability is calculated by
492 determining the 10% percentile result of the soil moisture datasets that are related to the occurred
493 landslides. The exceedance probability method is commonly utilised in landslide early warning
494 studies for calculating the rainfall-thresholds, which is therefore adopted here to examine its
495 performance for soil moisture threshold calculations.

496 To carry out the threshold evaluation, 45 rainfall events (during 2014-2015) are selected for the
497 purpose. The rainfall events are separated based on at least one-day of dry period (i.e., a period
498 without rainfall). The rainfall data from each rain gauge station is firstly combined using the
499 Thiessen Polygon method, and with visual analysis, the 45 events are then finally selected. The
500 information about the selected rainfall events can be found in Section 5. The threshold evaluation
501 is based on the statistical approach described in (Gariano et al., 2015;Zhuo et al., 2019), where soil
502 moisture threshold can be treated as a binary classifier of the soil moisture conditions that are likely
503 or unlikely to cause landslide events. With this hypothesis, the likelihood of a landslide event can
504 either be *true (T)* or *false (F)*, and the threshold forecasting can either be *positive (P)* or *negative*
505 *(N)*. The combinations of those four conditions can lead to four statistical outcomes (Figure 3a)
506 that are: *true positive (TP)*, *true negative (TN)*, *false positive (FP)*, and *false negative (FN)* (Wilks,
507 2011). Using the four outcomes, two statistical scores can be determined.

508 The Hit Rate (*HR*), which is the rate of the events that are correctly forecasted. Its formula is:

509
$$HR = \frac{TP}{TP+FN} \quad (1)$$

510 in the range of 0 and 1, with the best result as 1.

511 The False Alarm Rate (*FAR*), which is the rate of false alarms when the event did not occur. Its
512 formula is:

513
$$FAR = \frac{FP}{FP+TN} \quad (2)$$

514 in the range of 0 and 1, with the best result as 0.

515 For any soil moisture product, each threshold calculated is adopted to determine *T*, *F*, *P*, and *N*,
516 respectively. Those values are finally integrated to find the overall scores of *TP*, *FN*, *FP*, *TN*, *HR*,
517 and *FAR*. The threshold performance is then judged via the Receiver Operating Characteristic
518 (ROC) analysis (Hosmer and Lemeshow, 1989; Fawcett, 2006). As shown in Figure 3b, ROC curve
519 is based on *HR* against *FAR*, and each point in the curve represents a threshold scenario (i.e.,
520 selected exceedance probabilities). The optimal result (the red point) can only be realised when
521 the *HR* reaches 1 and the *FAR* reduces to 0. The closer the point to the red point, the better the
522 forecasting result is. To analyse and compare the forecasting performance numerically, the
523 Euclidean distances (*d*) for each scenario to the optimal point are computed.

524 **4. WRF Model Evaluations**

525 In this study, the evaluation is based on the daily mean soil moisture. The reason for not using the
526 antecedent soil moisture condition plus rainfall data on the day is because the purpose of this study
527 is to explore the relationship between different WRF simulated soil moisture and landslides solely.

528 In general, soil moisture is a predisposing factor for slope instability, while rainfall is the triggering
529 factor. The same rainfall may trigger or not a landslide depending on the soil moisture content at
530 the time of the rainfall event. The mean soil moisture on the day of the landslide implicitly account
531 for both the initial soil moisture and the effective rainfall absorbed by the ground, and can be a
532 robust indicator of the hydrological condition of the slope.

533 4.1 Soil Moisture Temporal Comparisons

534 Although there is only one soil moisture sensor that provides long-term soil moisture data in the
535 study region, it is still useful to compare it with the WRF estimated soil moisture. In this study, we
536 carry out a temporal comparison between all the three WRF soil moisture products with the in-situ
537 observations (at a single soil moisture measuring point in the plain area). The comparison is
538 implemented over the period from 2006 to 2015, and the WRF grid closest to the in-situ sensor
539 location is chosen. Figure 4 shows the comparison results at the four soil depths. The statistical
540 performance (correlation coefficient r and Root Mean Square Error $RMSE$) of the three LSM
541 schemes are summarised in Table 3. Based on the statistical results, Noah-MP surpasses other
542 schemes at most soil layers, except for Layer 2 where CLM4 shows stronger correlation and Layer
543 4 where Noah gives smaller $RMSE$ error. For Noah-MP, the best correlation is observed at the
544 surface layer (0.809), followed by the third (0.738), second (0.683) and fourth (0.498) layers; and
545 based on $RMSE$, the best performance is again observed at the surface layer and followed by the
546 second, third and fourth layers in sequence (as 0.060, 0.070, 0.088, and 0.092 m^3/m^3 , respectively).
547 From the temporal plots, it can be seen at all four soil layers, all three LSM schemes can produce
548 the soil moisture's seasonal cycle with most upward and downward trends successfully represented.
549 However, both the Noah and the CLM4 overestimate the variability at the upper two soil layers
550 during almost the whole study period, and the situation is the worst for the Noah. Comparatively,
551 the Noah-MP can better capture the wet soil moisture conditions especially at the surface layer;
552 and it is the only model of the three that is able to simulate the large soil drying phenomenon close
553 to the observations during the dry season, except for some extremely dry days. Towards 70 cm
554 depth, although Noah-MP is still able to capture most of the soil moisture variabilities during the
555 drying period, it significantly underestimates soil moisture values for most wet days. Similar

556 underestimation results can be observed for CLM4 and Noah during the wet season at 70 cm;
557 furthermore, both schemes are again not capable of reproducing the extremely drying phenomenon
558 and overestimate soil moisture for most of the dry season days. It is surprising to see that at the
559 deep soil layer (150 cm), all soil moisture products are underestimated, in particular, the outputs
560 from the CLM4 and the Noah-MP only show small fluctuations. However, the soil moisture
561 measurements from the in-situ sensor also get our attention as they show strange fluctuations with
562 numerous sudden drops and rise situations observed. The strange phenomenon is not expected at
563 such a deep soil layer (although groundwater capillary forces can increase the soil moisture, its
564 rate is normally very slow). One possible reason we suspect is due to sensor failure in the deep
565 zone. Therefore, the assessment result for the deep soil layer should be considered unreliable.
566 Overall for the Noah-MP, in addition to producing the highest correlation coefficient and the
567 lowest *RMSE*, its simulated soil moisture variations are the closest to the observations. The better
568 performance of the Noah-MP over the other two models agrees with the results found in (Cai et
569 al., 2014) (note: the paper uses standalone models, which are not coupled with WRF). Also, it has
570 been discussed in (Yang et al., 2011), the Noah MP presents a clear improvement over the Noah
571 in simulating soil moisture globally. However, it is noted the evaluation results are only based on
572 one soil moisture sensor located at the plain part of the study area.

573 **4.2 Rainfall Evaluations**

574 Since soil moisture is related to rainfall, it is useful to carry out the evaluations of WRF rainfall
575 estimations against the observations in the study area. The spatial plot of *R* for the three LSMs is
576 shown in Figure 5. It can be seen the performance of the three models are very close to each other,
577 with only small differences over the whole study region. In general, the performance is the best in
578 the Southeast region, with *R* reaches above 0.70. The poorest performance is observed in the

579 Northeast region and some parts of the mountain zone. Based on the spatial distribution of R , there
580 is no clear correlation between the WRF rainfall performance and the topography of the region.
581 The boxplot for the R performance is illustrated in Figure 6a. It can be seen again the performances
582 of the three models are very similar. Generally, R ranges between around 0.10 and 0.80, and with
583 the majority of the region performs around 0.40. $RMSE$ performance is also calculated. Similar to
584 the results of R , it has been found the $RMSE$ spatial distributions are very similar among the three
585 models. Therefore, the $RMSE$ spatial distribution map is not included in this paper. The boxplot of
586 the $RMSE$ is shown in Figure 6b. Generally, the $RMSE$ ranges between around 4 mm and 12 mm,
587 with some outliers between around 12 mm and 20 mm. Majority of the region performs at around
588 7 mm $RMSE$. The statistical calculations are summarised in Table 4. Based on the results of R and
589 $RMSE$, the WRF rainfall estimation performance in Emilia is similar to the one found in central
590 USA (Van Den Broeke et al., 2018).

591 **5. The Assessment of WRF Soil Moisture Threshold for Landslide Monitoring**

592 As introduced at the beginning of the paper, previous works (as discussed in the introduction
593 section) have demonstrated that in complex geomorphologic settings (e.g., in Emilia Romagna), a
594 rainfall threshold approach is too simple and more hydrologically driven approaches need to be
595 established. This section is to assess if the spatial distribution of soil moisture can provide useful
596 information for landslide monitoring at the regional scale. Particularly, all three soil moisture
597 products simulated through the WRF model are used to derive threshold models, and the
598 corresponding landslide prediction performances are then compared statistically. Here the
599 threshold is defined as the crucial soil moisture condition above which landslides are likely to
600 happen.

601 Among different factors for controlling the stability of slope, the slope angle is one of the most
602 critical ones. From the slope angle map in Figure 2, it can be seen the region has a clear spatial
603 pattern of high and low slope areas, with the majority of the high-slope areas (can be as steep as
604 around 40 degrees) located in the mountainous Southern part and the river valleys. Based on the
605 analysed events data, the landslides happened during the study period are mainly located in the
606 high-slope region, with a particularly high concentration around the central Southern part. The
607 spatial distribution of the landslide events is also in line with the overall geological characteristics
608 of the region, i.e., the Southern part mainly constitutes outcrop of sandstone rocks that make up
609 the steep slopes and are covered by a thin layer of permeable sandy soil, which are highly unstable.
610 Therefore, instead of only using one soil moisture threshold for the whole study area, it is useful
611 to divide the region into several slope groups so that within each group a threshold model is built.
612 To derive soil moisture threshold individually under different slope conditions, all data has been
613 divided into three groups based on the slope angle (0.4-1.86°; 1.87-9.61°; 9.52-40.43°; since no
614 landslide events are recorded under the 0-0.39° group, the group is not considered here), as results,
615 all groups have equal coverage areas. **There are different ways to group the slopes. In this study,**
616 **in order to have equal coverage areas, we have identified these class-break values.** ~~three groups~~
617 ~~have been defined with similar sizes so that relatively reliable results could be achieved from the~~
618 ~~statistical point of view.~~

619 In order to find the optimal threshold so that there are least missing alarms (i.e., threshold is
620 overestimated) and false alarms (i.e., threshold is underestimated), we test out 17 different
621 exceedance probabilities from 1% to 50%. For each LSM scheme, the total number of threshold
622 models is 204, which is the resultant of different combinations of slope groups, soil layers, and
623 exceedance probability conditions. The calculated thresholds for all LSM schemes under three

624 slope groups are plotted in Figure 7. Overall there is a clear trend between the slope angle and the
625 soil moisture threshold, that is with threshold becoming smaller for steeper areas. The correlation
626 is more evident at the upper three soil layers (i.e., the top 1 m depth of soil), with only a few
627 exceptions for Noah and CLM4 at the 1% and the 2% exceedance probabilities. At the deep soil
628 layer centred at 150 cm, the soil moisture threshold difference between Slope Group (S.G.) 2 and
629 3 becomes very small for all the three LSM schemes. This could be partially because at the deep
630 soil layer, the change of soil moisture is much smaller than at the surface layer, therefore the soil
631 moisture values for S.G. 2 and 3 could be too similar to differentiate. However, for milder slopes
632 (S.G. 1), the higher soil moisture triggering level always applies even down to the deepest soil
633 layer for all the three LSM schemes. In this study, the results show that wetter soil can trigger
634 landslides easier in milder slopes than in steeper slopes.

635 All the threshold models are then evaluated under the 45 selected rainfall events (Table 5) using
636 the ROC analysis. Each threshold determined for each of the slope class during the calibration is
637 used for the evaluation. The period of the selected rainfall events is between 1 day and 18 days,
638 and the average rainfall intensity ranges from 5.05 mm/day to 24.69 mm/day. The resultant
639 Euclidean distances (d) between each scenario of exceedance probability and the optimal point for
640 ROC analysis are listed in Table 6 for all three WRF LSM schemes at the tested exceedance
641 probabilities. The best performance (i.e., lowest d) in each column (i.e., each soil layer of an LSM
642 scheme) is highlighted. In addition, the d results are also plotted in Figure 8 to give a better view
643 of the overall trend amongst different soil layers and LSM schemes. From the figure, for all three
644 LSM schemes at all four soil layers, there is an overall downward and then stabilised trend. Overall
645 for Noah, the simulated surface layer soil moisture provides better landslide monitoring
646 performance than the rest of the soil layers from 1% to 35% exceedance probabilities; and the

647 scheme's worst performance is observed at the third soil layer centred at 70 cm. The values of d
648 for Noah's second and fourth layer are quite close to each other. For Noah-MP, the simulated
649 surface layer soil moisture gives the best performance amongst all four soil layers for most cases
650 between the 1% and 35% exceedance probability range; and the scheme's worst performance is
651 observed at the fourth layer. Unlike Noah, all four soil layers from the Noah-MP scheme provide
652 distinct performance amongst them (i.e., larger d difference). For CLM4, the performance for the
653 surface layer is quite similar to the second layer's, and the differences between the four layers are
654 small. From the Table 6, it can be seen for Noah the most suitable exceedance probabilities (i.e.,
655 the highlighted numbers) range between 35% to 50%; for Noah-MP they are between 30% and
656 50%, and for CLM4 it stays at 40% for all four soil layers. For both Noah and Noah-MP, the best
657 performance is observed at the surface layer ($d = 0.392$ and $d = 0.369$, respectively). ~~Furthermore,
658 the best performance for Noah and Noah MP follows a regular trend, that is the deeper the soil
659 layer, the poorer the landslide monitoring performance. There are several potential reasons for
660 such an outcome. First, the simulated soil moisture accuracy at the shallower layers are better than
661 the deeper zones. Second, although the wetness conditions at the sliding surface are important, the
662 soil moisture above it is also important (i.e., the loading should be heavier with more water in the
663 upper soil layer). Third, the region has very shallow landslides. Fourth, the WRF modelled soil
664 moisture is not accurate enough in assessing the landslide events in the study region. In order to
665 find out the extract reasons, comprehensive studies with more detailed landslide events datasets
666 are needed in future studies.~~ For CLM4, the best performances show no distinct pattern amongst
667 soil layers (i.e., with the best performance found at the soil Layer 3, followed by Layer 2, 1, and
668 4). Of all the LSM schemes and soil layers, the best performance is found for Noah-MP at the
669 surface layer with 30% exceedance probability ($d=0.369$). Based on the d results, WRF modelled

Commented [LZ1]: Moved to the Discussions

670 soil moisture provides better landslide prediction performance than the satellite ESA-CCI soil
671 moisture products as shown in our previous study ((Zhuo et al., 2019), i.e., $d = 0.51$). The ROC
672 curve for the Noah-MP scheme at the surface layer is shown in Figure 9. In the curve, each point
673 represents a scenario with a selected exceedance probability level. It is clear with various
674 exceedance probabilities, *FAR* can be decreased without sacrificing the *HR* score (e.g., 4% to 10%
675 exceedance probabilities). At the optimal point at the 30% exceedance probability, the best results
676 for *HR* and *FAR* are observed as 0.769 and 0.289, respectively.

677 **6. Discussions and Conclusion**

678 ~~In this study, the usability of WRF modelled soil moisture for landslide monitoring has been~~
679 ~~evaluated in the Emilia Romagna region based on the research duration between 2006 and 2015.~~
680 ~~Specifically, four layer soil moisture information simulated through the WRF's three most~~
681 ~~advanced LSM schemes (i.e., Noah, Noah-MP and CLM4) are compared for the purpose. Through~~
682 ~~the temporal comparison with the in-situ soil moisture observations, it has been found that all three~~
683 ~~LSM schemes at all four soil layers can produce the general soil moisture's seasonal cycle.~~
684 ~~However, only Noah-MP is able to simulate the large soil drying phenomenon close to the~~
685 ~~observations during the drying season, and it also gives the highest correlation coefficient and the~~
686 ~~lowest RMSE at most soil layers amongst the three LSM schemes. However, it should be noted,~~
687 ~~the soil moisture evaluation is only based on a single point based soil moisture sensor that is~~
688 ~~available in the plain region of the study area. Therefore, the WRF soil moisture performance over~~
689 ~~the whole study region, in particular, at the mountainous zone cannot be evaluated in this study.~~
690 ~~Since soil moisture is related to rainfall, we have carried out the WRF rainfall assessments, based~~
691 ~~on the comparison with the dense rainfall network in the region. The results have shown that there~~
692 ~~is no distinct difference between the three LSM schemes. The WRF rainfall performance is found~~

Commented [L22]: Moved to the Conclusions

693 ~~to be similar to a study carried out over the central USA. A landslide prediction model based on~~
694 ~~soil moisture and slope angle condition is built up. 17 various exceedance probably levels between~~
695 ~~1% and 50% are adopted to find the optimal threshold scenario. Through the ROC analysis of 612~~
696 ~~threshold models, the best performance is obtained by the Noah-MP at the surface soil layer with~~
697 ~~30% exceedance probability.~~

698 ~~It should be noted that weighting factors are not considered in the evaluation of the threshold~~
699 ~~models. Weighting factors can include both social and economic components, for instance, it can~~
700 ~~include the cost of a disaster event (e.g., both short term and long term impacts), the cost of the~~
701 ~~evacuation (e.g., relocation cost, business shut down), as well as the social impacts of both cases.~~
702 ~~In real life situations, the weighting could play important roles during the final decision making.~~
703 ~~As for instance, the damages resulted from a missing alarm event could be much more devastating~~
704 ~~than a false alarm event, or vice versa, and the situation also varies in different regions. Therefore,~~
705 ~~during operational applications, appropriate weighting factors should be considered.~~

706 ~~Furthermore, In this study, the best landslide prediction performance for Noah and Noah-MP~~
707 ~~follows a regular trend, that is the deeper the soil layer, the poorer the landslide monitoring~~
708 ~~performance. There are several potential reasons for such an outcome. First, the simulated soil~~
709 ~~moisture accuracy at the shallower layers are better than the deeper zones. Second, although the~~
710 ~~wetness conditions at the sliding surface are important, the soil moisture above it is also important~~
711 ~~(i.e., the loading should be heavier with more water in the upper soil layer). Third, the landslides~~
712 ~~occurred in the region are mainly in the top shallow soil layer. ~~the region has very shallow~~~~
713 ~~landslides. Fourth, the WRF modelled soil moisture is not accurate enough in assessing the~~
714 ~~landslide events in the study region. In order to find out the extract reasons, comprehensive studies~~
715 ~~with more detailed landslide events datasets are needed in future studies.~~

Commented [LZ3]: Moved from the results section

716 For the WRF soil moisture evaluation, clearly the evaluation work based on a single soil moisture
717 sensor located in plain area is not sufficient to make derive conclusions about the model's
718 performance over the whole study region. Therefore, the results are preliminary here. However,
719 in this study, by introducing the WRF spatial soil moisture information into the landslide prediction
720 model, the performance indeed has been improved in comparison with our previous study using
721 the satellite remote sensing soil moisture data (Zhuo et. al 2019). A similar concept has been
722 carried out by Segoni et al. (2018b), who implemented the soil moisture information simulated
723 from a hydrological model into a regional landslide early warning system with clear improvements
724 in false/ missing alarm performance. Although the results shown in this study is preliminary and
725 confined by the study area, the improved landslide prediction performance is already obtained.
726 Therefore, it is hoped with more densely soil moisture network data available globally and further
727 refinements of the method, the results could be improved further.

728 In addition, ideally, it will be useful if there is a dense soil moisture sensing network covering the
729 whole study area. In reality, that's not practical, so we have to rely on the spatial soil moisture
730 information by other means. So far, the soil moisture data with the best spatial and temporal
731 resolution is from the WRF model. A question is about how representative of a single soil moisture
732 sensor is for the whole study area. We have carried out the correlation study of a single sensor with
733 the whole study region (using the Noah-MP top-layer soil moisture data). As seen in Figure 10a,
734 the study region is divided into 44 equal-spacing grids (30 km apart), with the grid centres marked
735 as black crosses. The initial assumption is that the soil moisture sensor can only represent its
736 adjacent area, but the result was a surprise (Figure 10b). Based on the outcome, a single point
737 sensor can represent a significant proportion of the region. Admittedly, there are some areas where
738 the correlations are poor, in particular, the Grid 27, which has been compared with its surrounding

739 four grids as shown in Figure 11. It can be seen the soil moisture variation at Grid 27 is totally
740 different in comparison with the four surrounding grids'. The unique soil moisture variation pattern
741 observed in Grid 27 may be caused by different land use and soil type in that area, but clearly
742 further studies are needed to find out the exact reasons. The aforementioned work has prompt us
743 to a future study on the optimal soil moisture sensor network design for landside applications.
744 Although there are numerous studies on the rain gauge network design by the research community,
745 the soil moisture sensor network design has been largely ignored by the community. Hence, this
746 study has paved a foundation for such research.

747 For the WRF rainfall evaluations, the results are not good. Rainfall is one of the main drivers of
748 soil moisture change, and it is logical to think soil moisture and rainfall are highly linked, However,
749 since rainfall temporal vaiation is of high frequency data while soil moisture is of low frequency,
750 they behave differently. The results illustrate that for landslide study, it is better to use the WRF
751 soil moisture data than its rainfall data. Clearly more studies are needed to confirm this assumption.

752 ~~In this study, Here,~~ WRF is modelled based on the ERA-Interim datasets, however, it has been
753 found in ~~some studies~~Albergel et al. (2018), the performance of using the ERA5 has surpassed the
754 ERA-Interim. Therefore, the ERA5 datasets will be tested in our future studies. Model-based soil
755 moisture estimations could be affected by error accumulation issues, especially in the real-time
756 forecasting mode. A potential solution is to use data assimilation methodologies to correct such
757 errors by assimilating soil moisture information from other data sources. Since in-situ soil moisture
758 sensors are only sparsely available in limited regions, soil moisture measured via satellite remote
759 sensing technologies could provide useful alternatives. Another issue is with the landslide record
760 data, since most of them are based on human experiences (e.g., through newspapers, and victims),
761 a lot of incidences could be unreported. Therefore, the conclusion made here could be biased.

762 Other ways of expanding the current landslide catalog can depend on automatic landslide detection
763 methods based on remote sensing images (Nichol and Wong, 2005;Chen et al., 2018), internet
764 news (as all landslides with a relevant impact on society will be reported on internet news), and
765 automatic web data mining methods (Battistini et al., 2013;Goswami et al., 2018).

766 ~~In summary, this study provides an overview of the soil moisture performance of three WRF LSM
767 schemes for landslide hazard assessment. Based on the results, we demonstrate that the surface
768 soil moisture (centred at 10 cm) simulated through the Noah-MP LSM scheme is useful in
769 predicting landslide occurrences in the Emilia Romagna region. With the hitting rate of 0.769 and
770 the false alarm rate of 0.289 obtained in this study, such soil moisture information has the potential
771 in working with rainfall data to provide landslide predictions. However, one must bear in mind
772 that the results demonstrated in this study are only valid for the selected region. In order to make
773 a general conclusion, more researches are needed using the methodology described in this paper.
774 Particularly, a considerable number of catchments with a broad spectrum of climate and
775 environmental conditions will need to be investigated.~~

Commented [LZ5]: Moved to the Conclusions

776 7. Conclusions

777 In this study, the usability of WRF modelled soil moisture for landslide monitoring has been
778 evaluated in the Emilia Romagna region based on the research duration between 2006 and 2015.
779 Specifically, the four-layer soil moisture information simulated through the WRF's three most
780 advanced LSM schemes (i.e., Noah, Noah-MP and CLM4) is compared for the purpose. Through
781 the temporal comparison with the in-situ soil moisture observations, it has been found that all three
782 LSM schemes at all four soil layers can produce the general soil moisture's seasonal cycle.
783 However, only Noah-MP is able to simulate the large soil drying phenomenon close to the
784 observations during the drying season, and it also has the highest correlation coefficient and the

785 lowest RMSE at most soil layers amongst the three LSM schemes. However, it should be noted,
786 the soil moisture evaluation is only based on a single point-based soil moisture sensor that is
787 available in the plain region of the study area. Therefore, the WRF soil moisture performance over
788 the whole study region, in particular, at the mountainous zone cannot be evaluated in this study.
789 Since soil moisture is related to rainfall, we have carried out the WRF rainfall assessments, based
790 on the comparison with the dense rainfall network in the region. The results have shown that there
791 is no distinct difference between the three LSM schemes. The WRF rainfall performance is found
792 to be similar to a study carried out over the central USA (Van Den Broeke et al., 2018). A landslide
793 prediction model based on soil moisture and slope angle condition is built up. 17 various
794 exceedance probably levels between 1% and 50% are adopted to find the optimal threshold
795 scenario. Through the ROC analysis of 612 threshold models, the best performance is obtained by
796 the Noah-MP at the surface soil layer with 30% exceedance probability.

797 In summary, this study provides an overview of the soil moisture performance of three WRF LSM
798 schemes for landslide hazard assessment. Based on the results, we demonstrate that the surface
799 soil moisture (centred at 10 cm) simulated through the Noah-MP LSM scheme is useful in
800 predicting landslide occurrences in the Emilia Romagna region. With the hitting rate of 0.769 and
801 the false alarm rate of 0.289 obtained in this study, such soil moisture information has the potential
802 in working with rainfall data to provide landslide predictions. The further study on investigating
803 the soil moisture representation of a single soil moisture sensor over a large region has also been
804 carried out. The results demonstrate that although there is a significant elevation difference in the
805 region, a single soil moisture sensor has a high correlation with a significant proportion of the
806 study area. Although there are still a small proportion of areas where the correlation is poor, this

807 has prompt us to carry out a future study on the optimal design of soil moisture sensor network for
808 landslide study.

809 One must bear in mind that although the results demonstrated in this study are only valid for the
810 selected region, the methodology could be generalised to derive site-specific calibrations in other
811 sites using the proposed approach. In order to make a general conclusion, more researches are
812 needed using the methodology described in this paper. Particularly, a considerable number of
813 catchments with a broad spectrum of climate and environmental conditions and dense soil moisture
814 sensor network will need to be investigated.

815 **Acknowledgement**

816 This study is supported by Resilient Economy and Society by Integrated SysTems modelling
817 (RESIST), Newton Fund via Natural Environment Research Council (NERC) and Economic and
818 Social Research Council (ESRC) (NE/N012143/1), and the National Natural Science Foundation
819 of China (No: 4151101234). The Landslide inventory data is kindly provided by Dr Matteo Berti,
820 University of Bologna.

821 **References**

822 Albergel, C., Dutra, E., Munier, S., Calvet, J.-C., Munoz-Sabater, J., Rosnay, P. d., Balsamo, G. J.
823 H., and Sciences, E. S.: ERA-5 and ERA-Interim driven ISBA land surface model simulations:
824 which one performs better?, 22, 3515-3532, 2018.

825 Battistini, A., Segoni, S., Manzo, G., Catani, F., and Casagli, N. J. A. G.: Web data mining for
826 automatic inventory of geohazards at national scale, 43, 147-158, 2013.

827 Berry, P., Garlick, J., and Smith, R.: Near-global validation of the SRTM DEM using satellite
828 radar altimetry, Remote Sensing of Environment, 106, 17-27, 2007.

829 Berti, M., Martina, M., Franceschini, S., Pignone, S., Simoni, A., and Pizziolo, M.: Probabilistic
830 rainfall thresholds for landslide occurrence using a Bayesian approach, *Journal of Geophysical*
831 *Research: Earth Surface*, 117, 2012.

832 Bertolini, G., Guida, M., and Pizziolo, M. J. L.: Landslides in Emilia-Romagna region (Italy):
833 strategies for hazard assessment and risk management, 2, 302-312, 2005.

834 Bittelli, M., Valentino, R., Salvatorelli, F., and Pisa, P. R.: Monitoring soil-water and displacement
835 conditions leading to landslide occurrence in partially saturated clays, *Geomorphology*, 173, 161-
836 173, 2012.

837 Bogaard, T., and Greco, R.: Invited perspectives: Hydrological perspectives on precipitation
838 intensity-duration thresholds for landslide initiation: proposing hydro-meteorological thresholds,
839 *Natural Hazards and Earth System Sciences*, 18, 31-39, 2018.

840 Cai, X., Yang, Z. L., Xia, Y., Huang, M., Wei, H., Leung, L. R., and Ek, M. B.: Assessment of
841 simulated water balance from Noah, Noah-MP, CLM, and VIC over CONUS using the NLDAS
842 test bed, *Journal of Geophysical Research: Atmospheres*, 119, 13,751-713,770, 2014.

843 Cai, X.: Hydrological assessment and biogeochemical advancement of the Noah-MP land surface
844 model, Doctor of Philosophy, Geological Sciences, The University of Texas at Austin, 164 pp.,
845 2015.

846 Chae, B.-G., Park, H.-J., Catani, F., Simoni, A., and Berti, M.: Landslide prediction, monitoring
847 and early warning: a concise review of state-of-the-art, *Geosciences Journal*, 21, 1033-1070, 2017.

848 Chen, F., and Dudhia, J.: Coupling an advanced land surface-hydrology model with the Penn State-
849 NCAR MM5 modeling system. Part I: Model implementation and sensitivity, *Monthly Weather*
850 *Review*, 129, 569-585, 2001.

851 Chen, Z., Zhang, Y., Ouyang, C., Zhang, F., and Ma, J. J. S.: Automated landslides detection for
852 mountain cities using multi-temporal remote sensing imagery, 18, 821, 2018.

853 Ciabatta, L., Camici, S., Brocca, L., Ponziani, F., Stelluti, M., Berni, N., and Moramarco, T. J. J.
854 o. H.: Assessing the impact of climate-change scenarios on landslide occurrence in Umbria Region,
855 *Italy*, 541, 285-295, 2016.

856 Crozier, M. J.: Prediction of rainfall-triggered landslides: A test of the antecedent water status
857 model, *Earth surface processes and landforms*, 24, 825-833, 1999.

858 Dee, D. P., Uppala, S. M., Simmons, A., Berrisford, P., Poli, P., Kobayashi, S., Andrae, U.,
859 Balmaseda, M., Balsamo, G., and Bauer, d. P.: The ERA-Interim reanalysis: Configuration and
860 performance of the data assimilation system, *Quarterly Journal of the royal meteorological society*,
861 137, 553-597, 2011.

862 Dorigo, W., Wagner, W., Albergel, C., Albrecht, F., Balsamo, G., Brocca, L., Chung, D., Ertl, M.,
863 Forkel, M., and Gruber, A.: ESA CCI Soil Moisture for improved Earth system understanding:
864 State-of-the art and future directions, *Remote Sensing of Environment*, 203, 185-215, 2017.

865 Dudhia, J.: Numerical study of convection observed during the winter monsoon experiment using
866 a mesoscale two-dimensional model, *Journal of the Atmospheric Sciences*, 46, 3077-3107, 1989.

867 Ek, M., Mitchell, K., Lin, Y., Rogers, E., Grunmann, P., Koren, V., Gayno, G., and Tarpley, J.:
868 Implementation of Noah land surface model advances in the National Centers for Environmental
869 Prediction operational mesoscale Eta model, *Journal of Geophysical Research: Atmospheres*, 108,
870 2003.

871 Fawcett, T.: An introduction to ROC analysis, *Pattern recognition letters*, 27, 861-874, 2006.

872 Gao, Q., Zribi, M., Escorihuela, M., and Baghdadi, N. J. S.: Synergetic use of Sentinel-1 and
873 Sentinel-2 data for soil moisture mapping at 100 m resolution, 17, 1966, 2017.

874 Gariano, S. L., Brunetti, M. T., Iovine, G., Melillo, M., Peruccacci, S., Terranova, O., Vennari, C.,
875 and Guzzetti, F.: Calibration and validation of rainfall thresholds for shallow landslide forecasting
876 in Sicily, southern Italy, *Geomorphology*, 228, 653-665, 2015.

877 Geudtner, D., Torres, R., Snoeij, P., Davidson, M., and Rommen, B.: Sentinel-1 system capabilities
878 and applications, 2014 IEEE Geoscience and Remote Sensing Symposium, 2014, 1457-1460,

879 Gilliland, E. K., and Rowe, C. M.: A comparison of cumulus parameterization schemes in the
880 WRF model, *Proceedings of the 87th AMS Annual Meeting & 21th Conference on Hydrology*,
881 2007,

882 Glade, T., Crozier, M., and Smith, P.: Applying probability determination to refine landslide-
883 triggering rainfall thresholds using an empirical “Antecedent Daily Rainfall Model”, *Pure and*
884 *Applied Geophysics*, 157, 1059-1079, 2000.

885 Goswami, S., Chakraborty, S., Ghosh, S., Chakrabarti, A., and Chakraborty, B. J. A. S. E. J.: A
886 review on application of data mining techniques to combat natural disasters, 9, 365-378, 2018.

887 Greve, P., Warrach-Sagi, K., and Wulfmeyer, V.: Evaluating soil water content in a WRF-Noah
888 downscaling experiment, *Journal of Applied Meteorology and Climatology*, 52, 2312-2327, 2013.

889 Hawke, R., and McConchie, J.: In situ measurement of soil moisture and pore-water pressures in
890 an ‘incipient’ landslide: Lake Tutira, New Zealand, *Journal of environmental management*, 92,
891 266-274, 2011.

892 Hong, S.-Y., Noh, Y., and Dudhia, J.: A new vertical diffusion package with an explicit treatment
893 of entrainment processes, *Monthly Weather Review*, 134, 2318-2341, 2006.

894 Hosmer, D., and Lemeshow, S.: *Applied logistic regression*. 1989, New York: Johns Wiley & Sons,
895 1989.

896 Jiménez, P. A., Dudhia, J., González-Rouco, J. F., Navarro, J., Montávez, J. P., and García-
897 Bustamante, E.: A revised scheme for the WRF surface layer formulation, *Monthly Weather*
898 *Review*, 140, 898-918, 2012.

899 Jordan, R.: A one-dimensional temperature model for a snow cover: Technical documentation for
900 SNTHERM. 89, Cold Regions Research and Engineering Laboratory, 1991.

901 Kain, J. S.: The Kain-Fritsch convective parameterization: An update, *Journal of Applied*
902 *Meteorology*, 43, [http://dx.doi.org/10.1175/1520-0450\(2004\)043<0170:TKCPAU>2.0.CO;2](http://dx.doi.org/10.1175/1520-0450(2004)043<0170:TKCPAU>2.0.CO;2),
903 2004.

904 Klose, M., Highland, L., Damm, B., and Terhorst, B.: Estimation of Direct Landslide Costs in
905 Industrialized Countries: Challenges, Concepts, and Case Study, in: *Landslide Science for a Safer*
906 *Geoenvironment*, World Landslide Forum 3, China (Beijing), 2014, 661-667,

907 Lagomarsino, D., Segoni, S., Fanti, R., and Catani, F. J. L.: Updating and tuning a regional-scale
908 landslide early warning system, 10, 91-97, 2013.

909 Lagomarsino, D., Segoni, S., Rosi, A., Rossi, G., Battistini, A., Catani, F., Casagli, N. J. N. H.,
910 and Sciences, E. S.: Quantitative comparison between two different methodologies to define
911 rainfall thresholds for landslide forecasting, 15, 2413-2423, 2015.

912 Lawrence, D. M., and Slater, A. G.: Incorporating organic soil into a global climate model, *Climate*
913 *Dynamics*, 30, 145-160, 2008.

914 Lawrence, D. M., Oleson, K. W., Flanner, M. G., Thornton, P. E., Swenson, S. C., Lawrence, P.
915 J., Zeng, X., Yang, Z. L., Levis, S., and Sakaguchi, K.: Parameterization improvements and
916 functional and structural advances in version 4 of the Community Land Model, *Journal of*
917 *Advances in Modeling Earth Systems*, 3, 27, 2011.

918 Lawrence, D. M., Oleson, K. W., Flanner, M. G., Fletcher, C. G., Lawrence, P. J., Levis, S.,
919 Swenson, S. C., and Bonan, G. B.: The CCSM4 land simulation, 1850–2005: Assessment of
920 surface climate and new capabilities, *Journal of Climate*, 25, 2240-2260, 2012.

921 Leung, L. R., and Qian, Y.: Atmospheric rivers induced heavy precipitation and flooding in the
922 western US simulated by the WRF regional climate model, *Geophysical research letters*, 36, 2009.

923 Liang, X., Xie, Z., and Huang, M.: A new parameterization for surface and groundwater
924 interactions and its impact on water budgets with the variable infiltration capacity (VIC) land
925 surface model, *Journal of Geophysical Research: Atmospheres*, 108, 2003.

926 Maheu, A., Anctil, F., Gaborit, É., Fortin, V., Nadeau, D. F., and Therrien, R.: A field evaluation
927 of soil moisture modelling with the Soil, Vegetation, and Snow (SVS) land surface model using
928 evapotranspiration observations as forcing data, *Journal of Hydrology*, 558, 532-545, 2018.

929 Martelloni, G., Segoni, S., Fanti, R., and Catani, F. J. L.: Rainfall thresholds for the forecasting of
930 landslide occurrence at regional scale, 9, 485-495, 2012.

931 Mlawer, E. J., Taubman, S. J., Brown, P. D., Iacono, M. J., and Clough, S. A.: Radiative transfer
932 for inhomogeneous atmospheres: RRTM, a validated correlated-k model for the longwave, *Journal*
933 *of Geophysical Research: Atmospheres*, 102, 16663-16682, 1997.

934 Weather research and forecasting model, 2018.

935 Nichol, J., and Wong, M. J. I. j. o. r. s.: Satellite remote sensing for detailed landslide inventories
936 using change detection and image fusion, 26, 1913-1926, 2005.

937 Niu, G. Y., Yang, Z. L., Dickinson, R. E., and Gulden, L. E.: A simple TOPMODEL-based runoff
938 parameterization (SIMTOP) for use in global climate models, *Journal of Geophysical Research:
939 Atmospheres*, 110, 2005.

940 Niu, G. Y., Yang, Z. L., Dickinson, R. E., Gulden, L. E., and Su, H.: Development of a simple
941 groundwater model for use in climate models and evaluation with Gravity Recovery and Climate
942 Experiment data, *Journal of Geophysical Research: Atmospheres*, 112, 2007.

943 Niu, G. Y., Yang, Z. L., Mitchell, K. E., Chen, F., Ek, M. B., Barlage, M., Kumar, A., Manning,
944 K., Niyogi, D., and Rosero, E.: The community Noah land surface model with
945 multiparameterization options (Noah-MP): 1. Model description and evaluation with local-scale
946 measurements, *Journal of Geophysical Research: Atmospheres*, 116, 2011.

947 Oleson, K., Niu, G. Y., Yang, Z. L., Lawrence, D., Thornton, P., Lawrence, P., Stöckli, R.,
948 Dickinson, R., Bonan, G., and Levis, S.: Improvements to the Community Land Model and their
949 impact on the hydrological cycle, *Journal of Geophysical Research: Biogeosciences (2005–2012)*,
950 113, 2008.

951 Oleson, K. W., Lawrence, D. M., Gordon, B., Flanner, M. G., Kluzek, E., Peter, J., Levis, S.,
952 Swenson, S. C., Thornton, E., and Feddema, J.: Technical description of version 4.0 of the
953 Community Land Model (CLM), 2010.

954 Paloscia, S., Pettinato, S., Santi, E., Notarnicola, C., Pasolli, L., and Reppucci, A. J. R. S. o. E.:
955 Soil moisture mapping using Sentinel-1 images: Algorithm and preliminary validation, 134, 234-
956 248, 2013.

957 Pistocchi, A., Bouraoui, F., and Bittelli, M.: A simplified parameterization of the monthly topsoil
958 water budget, *Water Resources Research*, 44, 2008.

959 Ponziani, F., Pandolfo, C., Stelluti, M., Berni, N., Brocca, L., and Moramarco, T. J. L.: Assessment
960 of rainfall thresholds and soil moisture modeling for operational hydrogeological risk prevention
961 in the Umbria region (central Italy), 9, 229-237, 2012.

962 Posner, A. J., and Georgakakos, K. P.: Soil moisture and precipitation thresholds for real-time
963 landslide prediction in El Salvador, *Landslides*, 12, 1179-1196, 2015.

964 Rossi, M., Witt, A., Guzzetti, F., Malamud, B. D., Peruccacci, S. J. E. S. P., and Landforms:
965 Analysis of historical landslide time series in the Emilia-Romagna region, northern Italy, 35, 1123-
966 1137, 2010.

967 Segoni, S., Lagomarsino, D., Fanti, R., Moretti, S., and Casagli, N.: Integration of rainfall
968 thresholds and susceptibility maps in the Emilia Romagna (Italy) regional-scale landslide warning
969 system, *Landslides*, 12, 773-785, 2015.

970 Segoni, S., Rosi, A., Fanti, R., Gallucci, A., Monni, A., and Casagli, N. J. W.: A Regional-Scale
971 Landslide Warning System Based on 20 Years of Operational Experience, 10, 1297, 2018a.

972 Segoni, S., Rosi, A., Lagomarsino, D., Fanti, R., and Casagli, N.: Brief communication: Using
973 averaged soil moisture estimates to improve the performances of a regional-scale landslide early
974 warning system, *Natural Hazards and Earth System Sciences*, 18, 807-812, 2018b.

975 Skamarock, W., Klemp, J., Dudhia, J., Gill, D., Barker, D., Duda, M., Huang, X., Wang, W., and
976 Powers, J.: A description of the advanced research WRF Version 3, NCAR technical note,
977 Mesoscale and Microscale Meteorology Division, National Center for Atmospheric Research,
978 Boulder, Colorado, USA, 2008.

979 Skamarock, W. C., Klemp, J. B., Dudhia, J., Gill, D. O., Barker, D. M., Wang, W., and Powers, J.
980 G.: A description of the advanced research WRF version 2, National Center For Atmospheric
981 Research Boulder Co Mesoscale and Microscale Meteorology Div, 2005.

982 Srivastava, P. K., Han, D., Rico-Ramirez, M. A., Al-Shrafany, D., and Islam, T.: Data fusion
983 techniques for improving soil moisture deficit using SMOS satellite and WRF-NOAH land surface
984 model, *Water resources management*, 27, 5069-5087, 2013a.

985 Srivastava, P. K., Han, D., Rico Ramirez, M. A., and Islam, T.: Comparative assessment of
986 evapotranspiration derived from NCEP and ECMWF global datasets through Weather Research
987 and Forecasting model, *Atmospheric Science Letters*, 14, 118-125, 2013b.

988 Srivastava, P. K., Han, D., Rico-Ramirez, M. A., O'Neill, P., Islam, T., Gupta, M., and Dai, Q.:
989 Performance evaluation of WRF-Noah Land surface model estimated soil moisture for

990 hydrological application: Synergistic evaluation using SMOS retrieved soil moisture, *Journal of*
991 *Hydrology*, 529, 200-212, 2015.

992 Stéfanon, M., Drobinski, P., D'Andrea, F., Lebeaupin-Brossier, C., and Bastin, S.: Soil moisture-
993 temperature feedbacks at meso-scale during summer heat waves over Western Europe, *Climate*
994 *dynamics*, 42, 1309-1324, 2014.

995 Temimi, M., Leconte, R., Chaouch, N., Sukumal, P., Khanbilvardi, R., and Brissette, F.: A
996 combination of remote sensing data and topographic attributes for the spatial and temporal
997 monitoring of soil wetness, *Journal of Hydrology*, 388, 28-40, 2010.

998 Thompson, G., Field, P. R., Rasmussen, R. M., and Hall, W. D.: Explicit forecasts of winter
999 precipitation using an improved bulk microphysics scheme. Part II: Implementation of a new snow
1000 parameterization, *Monthly Weather Review*, 136, 5095-5115, 2008.

1001 Tsai, T.-L., and Chen, H.-F.: Effects of degree of saturation on shallow landslides triggered by
1002 rainfall, *Environmental Earth Sciences*, 59, 1285-1295, 2010.

1003 Valenzuela, P., Domínguez-Cuesta, M. J., García, M. A. M., and Jiménez-Sánchez, M.: Rainfall
1004 thresholds for the triggering of landslides considering previous soil moisture conditions (Asturias,
1005 NW Spain), *Landslides*, 15, 273-282, 2018.

1006 Van Den Broeke, M. S., Kalin, A., Alavez, J. A. T., Oglesby, R., Hu, Q. J. T., and climatology, a.:
1007 A warm-season comparison of WRF coupled to the CLM4. 0, Noah-MP, and Bucket hydrology
1008 land surface schemes over the central USA, 134, 801-816, 2018.

1009 Wei, J., Dirmeyer, P. A., Guo, Z., Zhang, L., and Misra, V.: How much do different land models
1010 matter for climate simulation? Part I: Climatology and variability, *Journal of Climate*, 23, 3120-
1011 3134, 2010.

1012 Wharton, S., Simpson, M., Osuna, J., Newman, J., and Biraud, S.: Assessment of Land Surface
1013 Model Performance in WRF for Simulating Wind at Heights Relevant to the Wind Energy
1014 Community, Lawrence Livermore National Lab (LLNL), Livermore, CA (United States), 2013.

1015 Wilks, D.: *Statistical Methods in the Atmospheric Sciences*, 3rd ed., Academic Press, 2011.

1016 Yang, Z. L., Niu, G. Y., Mitchell, K. E., Chen, F., Ek, M. B., Barlage, M., Longuevergne, L.,
1017 Manning, K., Niyogi, D., and Tewari, M.: The community Noah land surface model with
1018 multiparameterization options (Noah-MP): 2. Evaluation over global river basins, *Journal of*
1019 *Geophysical Research: Atmospheres*, 116, 2011.

1020 Zaidi, S. M., and Gisen, J. I. A.: Evaluation of Weather Research and Forecasting (WRF)
1021 Microphysics single moment class-3 and class-6 in Precipitation Forecast, *MATEC Web of*
1022 *Conferences*, 2018, 03007,

1023 Zaitchik, B. F., Santanello, J. A., Kumar, S. V., and Peters-Lidard, C. D.: Representation of soil
1024 moisture feedbacks during drought in NASA unified WRF (NU-WRF), *Journal of*
1025 *Hydrometeorology*, 14, 360-367, 2013.

1026 Zeng, X., and Decker, M.: Improving the numerical solution of soil moisture-based Richards
1027 equation for land models with a deep or shallow water table, *Journal of Hydrometeorology*, 10,
1028 308-319, 2009.

1029 Zhao, B., Dai, Q., Han, D., Dai, H., Mao, J., and Zhuo, L.: Antecedent wetness and rainfall
1030 information in landslide threshold definition, *Hydrol. Earth Syst. Sci. Discuss.*, 2019, 1-26,
1031 10.5194/hess-2019-150, 2019a.

1032 Zhao, B., Dai, Q., Han, D., Dai, H., Mao, J., and Zhuo, L. J. J. o. H.: Probabilistic thresholds for
1033 landslides warning by integrating soil moisture conditions with rainfall thresholds, 574, 276-287,
1034 2019b.

1035 Zhuo, L., Dai, Q., and Han, D.: Evaluation of SMOS soil moisture retrievals over the central United
1036 States for hydro-meteorological application, *Physics and Chemistry of the Earth, Parts A/B/C*, 83,
1037 146-155, 2015a.

1038 Zhuo, L., Han, D., Dai, Q., Islam, T., and Srivastava, P. K.: Appraisal of NLDAS-2 multi-model
1039 simulated soil moistures for hydrological modelling, *Water resources management*, 29, 3503-3517,
1040 2015b.

1041 Zhuo, L., Dai, Q., Han, D., Chen, N., Zhao, B., and Berti, M.: Evaluation of remotely sensed soil
1042 moisture for landslide hazard assessment, *IEEE Journal of Selected Topics in Applied Earth*
1043 *Observations and Remote Sensing*, 12, 162 - 173, 2019.

1044

Table 1. Comparison of Noah, Noah-MP, and CLM4.

	Noah	Noah-MP	CLM4
Energy balance	Yes	Yes	Yes
Water balance	Yes	Yes	Yes
No. of soil layers	4	4	10
Depth of total soil column	2.0 m	2.0 m	3.802 m
Model soil layer thickness	0.1, 0.3, 0.6, 1.0 m	0.1, 0.3, 0.6, 1.0 m	0.018, 0.028, 0.045, 0.075, 0.124, 0.204, 0.336, 0.553, 0.913, 1.506 m
No. of vegetation layers	A single combined surface layer of vegetation and snow	Single layer	Single layer
Vegetation	Dominant vegetation type in one grid cell with prescribed LAI	Dominant vegetation type in one grid cell with dynamic LAI	Up to 10 vegetation types in one grid cell with prescribed LAI
No. of snow layers	A single combined surface layer of vegetation and snow	Up to three layers	Up to five layers

Table 2. WRF parameterizations used in this study.

	Settings/ Parameterizations	References
Map projection	Lambert	
Central point of domain	Latitude: 44.54; Longitude: 11.02	
Latitudinal grid length	5 km	
Longitudinal grid length	5 km	
Model output time step	Daily	
Nesting	Two-way	
Land surface model	Noah, Noah-MP, CLM	
Simulation period	1/1/2006 – 31/12/2015	
Spin-up period	1/1/2005 – 31/12/2005	
Microphysics	New Thompson	(Thompson et al., 2008)
Shortwave radiation	Dudhia scheme	(Dudhia, 1989)
Longwave radiation	Rapid Radiative Transfer Model	(Mlawer et al., 1997)
Surface layer	Revised MM5	(Jiménez et al., 2012; Chen and Dudhia, 2001)
Planetary boundary layer	Yonsei University method	(Hong et al., 2006)
Cumulus Parameterization	Kain-Fritsch (new Eta) scheme	(Kain, 2004)

Table 3. Statistical summary of the WRF performance in simulating soil moisture for different soil layers, based on comparison with the single point in-situ observations.

	<i>R</i>				<i>RMSE (m³/m³)</i>			
	0.10 m	0.25 m	0.70 m	1.50 m	0.1 m	0.25 m	0.70 m	1.50 m
Noah	0.728	0.645	0.660	0.430	0.123	0.125	0.141	0.055
Noah-MP	0.809	0.683	0.738	0.498	0.060	0.070	0.088	0.092
CLM	0.789	0.743	0.648	0.287	0.089	0.087	0.123	0.089

Table 4 Statistical summary of the WRF performance in simulating rainfall for the whole study region, based on comparison with the in-situ rainfall network.

	<i>R</i>			<i>RMSE (mm)</i>		
	Noah	Noah-MP	CLM4	Noah	Noah-MP	CLM4
Min	0.094	0.090	0.076	4.275	4.286	4.219
Max	0.779	0.798	0.801	19.814	19.178	19.476
Mean	0.425	0.426	0.421	7.772	7.719	7.943
0.25 percentile	0.147	0.130	0.154	4.579	4.297	4.438
0.50 percentile	0.189	0.153	0.210	4.951	4.909	4.910
0.75 percentile	0.192	0.183	0.211	5.006	4.970	5.010

Table 5. Rainfall events information.

Starting date			Ending date			Duration (days)	Rainfall intensity (mm/day)	Number of Landslide events
Year	Month	Day	Year	Month	Day			
2014	1	13	2014	1	24	12	20.50	2
2014	1	28	2014	2	14	18	13.61	0
2014	2	26	2014	3	6	9	13.35	0
2014	3	22	2014	3	27	6	11.08	0
2014	4	4	2014	4	5	2	18.98	0
2014	4	27	2014	5	4	8	12.13	0
2014	5	26	2014	6	3	9	5.05	0
2014	6	14	2014	6	16	3	18.29	0
2014	6	25	2014	6	30	6	11.39	0
2014	7	7	2014	7	14	8	7.84	0
2014	7	21	2014	7	30	10	15.35	0
2014	8	31	2014	9	5	6	5.67	0
2014	9	10	2014	9	12	3	11.84	0
2014	9	19	2014	9	20	2	23.04	0
2014	10	1	2014	10	1	1	14.51	0
2014	10	10	2014	10	17	8	13.01	0
2014	11	4	2014	11	18	15	18.28	0
2014	11	25	2014	12	7	13	7.58	0
2014	12	13	2014	12	16	4	6.24	0
2015	1	16	2015	1	17	2	14.87	0
2015	1	21	2015	1	23	3	7.13	0
2015	1	29	2015	2	10	13	9.98	0
2015	2	13	2015	2	17	5	6.62	1
2015	2	21	2015	2	26	6	11.84	4
2015	3	3	2015	3	7	5	11.69	1
2015	3	15	2015	3	17	3	9.00	0
2015	3	21	2015	3	27	7	12.09	2
2015	4	3	2015	4	5	3	16.62	0
2015	4	17	2015	4	18	2	6.99	0
2015	4	26	2015	4	29	4	11.23	0
2015	5	15	2015	5	16	2	8.83	0
2015	5	20	2015	5	27	8	10.58	1
2015	6	8	2015	6	11	4	6.47	0
2015	6	16	2015	6	19	4	13.44	0
2015	6	23	2015	6	24	2	6.07	0
2015	7	22	2015	7	25	4	6.05	0
2015	8	9	2015	8	10	2	24.69	0
2015	8	15	2015	8	19	5	10.69	0
2015	8	23	2015	8	24	2	7.88	0
2015	9	13	2015	9	14	2	24.66	1
2015	9	23	2015	9	24	2	7.50	0
2015	10	1	2015	10	7	7	13.73	0
2015	10	10	2015	10	19	10	9.40	0
2015	10	27	2015	10	29	3	20.33	0
2015	11	21	2015	11	25	5	13.78	1

Table 6. Results of Euclidean distances (d) between individual points and the optimal point for ROC analysis are listed. The best performance (i.e., lowest d) for each column (i.e., each soil layer of an LSM scheme) is highlighted. The optimal performance of all is highlighted in red.

$e.p.$ (%)	Noah				Noah-MP				CLM4			
	10 cm	25 cm	70 cm	150 cm	10 cm	25 cm	70 cm	150 cm	10 cm	25 cm	70 cm	150 cm
1	0.942	0.971	0.962	0.947	0.857	0.937	0.897	0.963	0.942	0.939	0.978	0.975
2	0.906	0.945	0.963	0.923	0.854	0.912	0.883	0.959	0.923	0.922	0.959	0.952
3	0.889	0.924	0.961	0.915	0.849	0.855	0.838	0.952	0.870	0.874	0.940	0.947
4	0.884	0.898	0.946	0.914	0.838	0.814	0.829	0.924	0.831	0.843	0.925	0.947
5	0.860	0.875	0.924	0.896	0.820	0.793	0.812	0.908	0.791	0.822	0.915	0.921
6	0.835	0.854	0.910	0.874	0.803	0.785	0.800	0.905	0.770	0.817	0.911	0.909
7	0.827	0.861	0.902	0.858	0.777	0.767	0.791	0.889	0.753	0.801	0.902	0.900
8	0.816	0.849	0.889	0.851	0.745	0.765	0.782	0.876	0.745	0.785	0.902	0.910
9	0.790	0.827	0.878	0.834	0.706	0.732	0.766	0.871	0.742	0.777	0.864	0.904
10	0.762	0.811	0.863	0.825	0.672	0.702	0.747	0.862	0.738	0.767	0.835	0.887
15	0.615	0.741	0.839	0.763	0.560	0.629	0.716	0.835	0.702	0.700	0.729	0.790
20	0.485	0.627	0.779	0.652	0.515	0.571	0.624	0.774	0.570	0.602	0.594	0.650
25	0.432	0.544	0.728	0.512	0.403	0.465	0.574	0.736	0.509	0.522	0.471	0.509
30	0.437	0.495	0.643	0.451	0.369	0.375	0.544	0.679	0.475	0.477	0.447	0.469
35	0.392	0.446	0.592	0.436	0.390	0.404	0.411	0.498	0.441	0.435	0.428	0.430
40	0.500	0.407	0.531	0.416	0.439	0.385	0.382	0.436	0.406	0.405	0.398	0.410
50	0.552	0.425	0.404	0.411	0.489	0.417	0.416	0.429	0.437	0.435	0.408	0.437

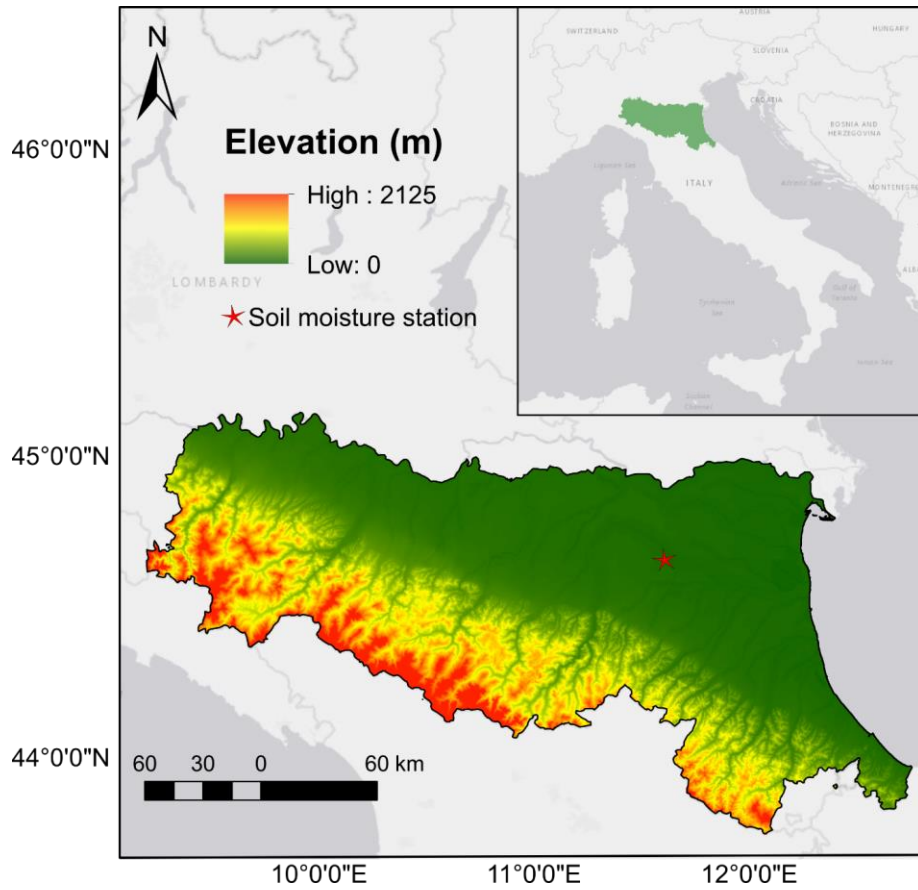


Figure 1. Location of the Emilia Romagna Region with elevation map and in-situ soil moisture station also shown.

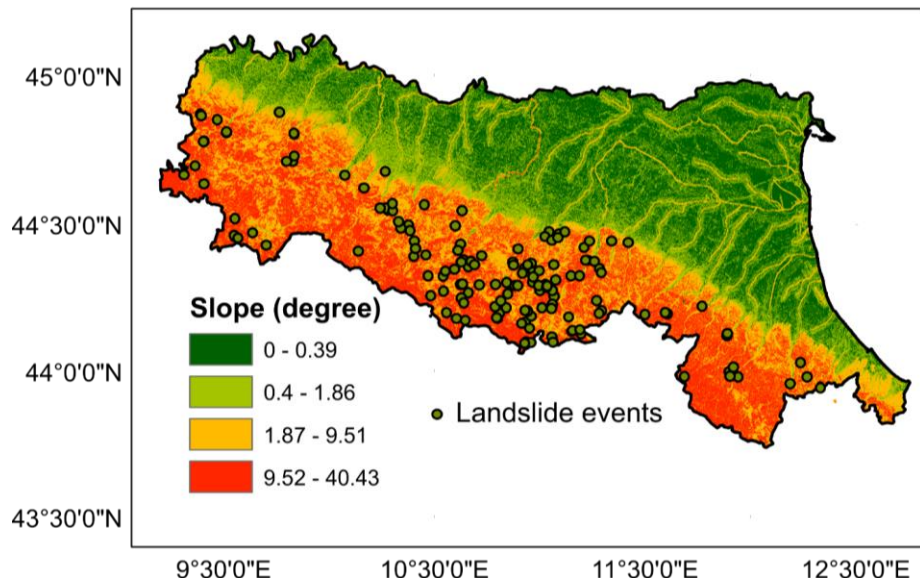


Figure 2. Landslide events with slope angle map.

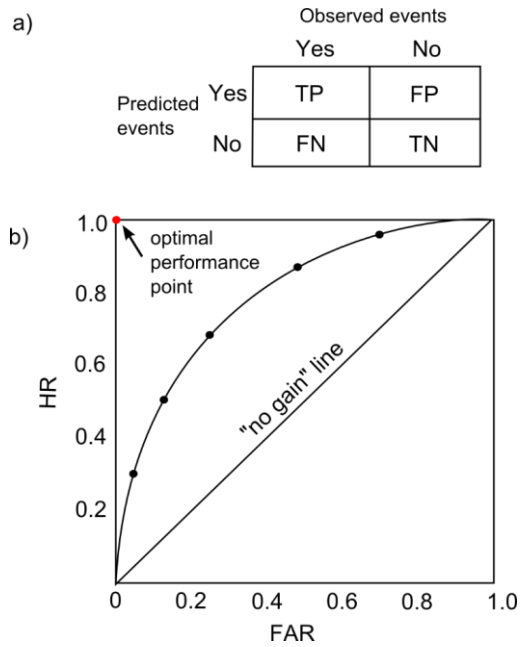


Figure 3. a) Contingency table illustrates the four possible outcomes of a binary classifier model: TP (True Positive), TN (True Negative), FP (False Positive), and FN (False Negative). b) ROC (Receiver Operating Characteristic) analysis with HR (Hitting Rate) against FAR (False Alarm Rate).

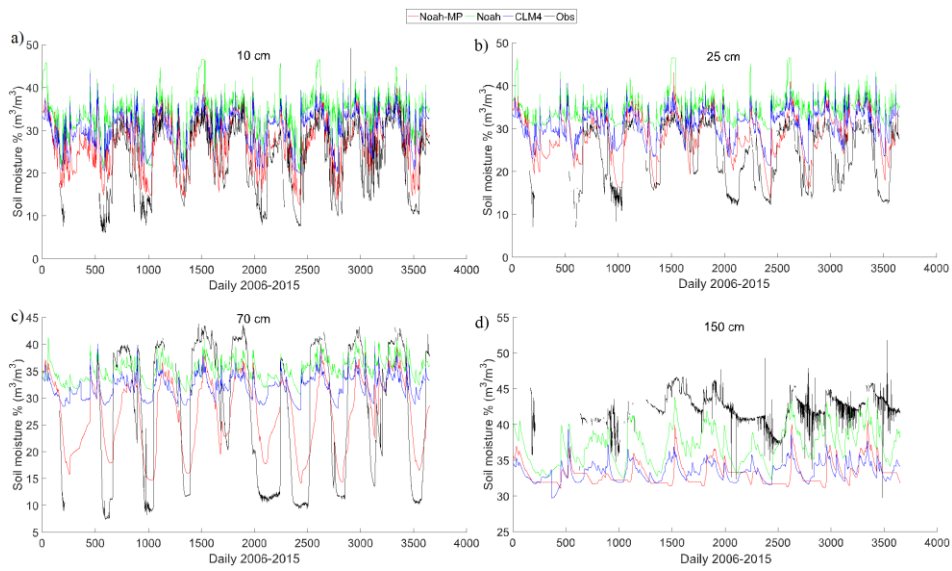


Figure 4. Soil moisture temporal variations of WRF simulations and in-situ observations for four soil layers at a) 10 cm; b) 25 cm; c) 70 cm; and d) 150 cm.

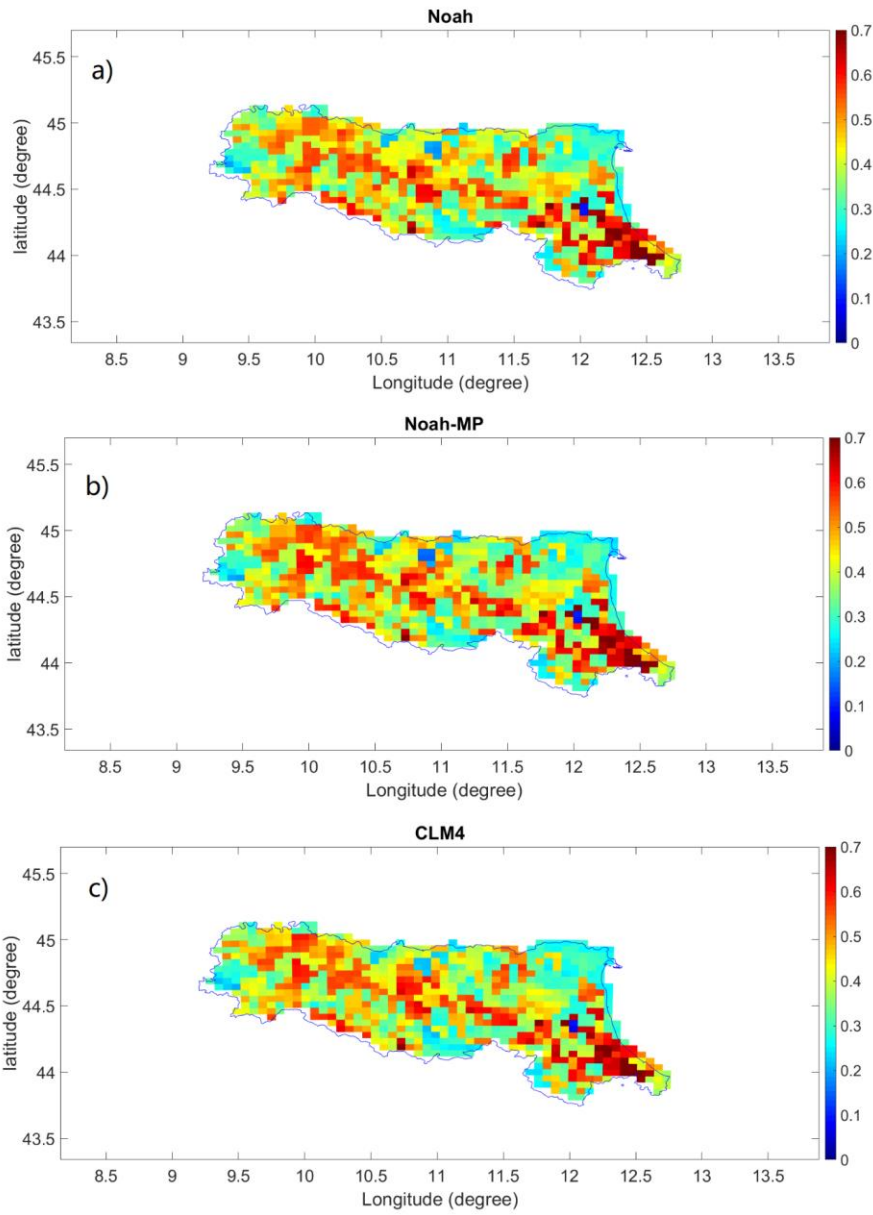


Figure 5. Rainfall evaluation: spatial distribution of the correlation coefficient R of a) Noah, b) Noah-MP and c) CLM4.

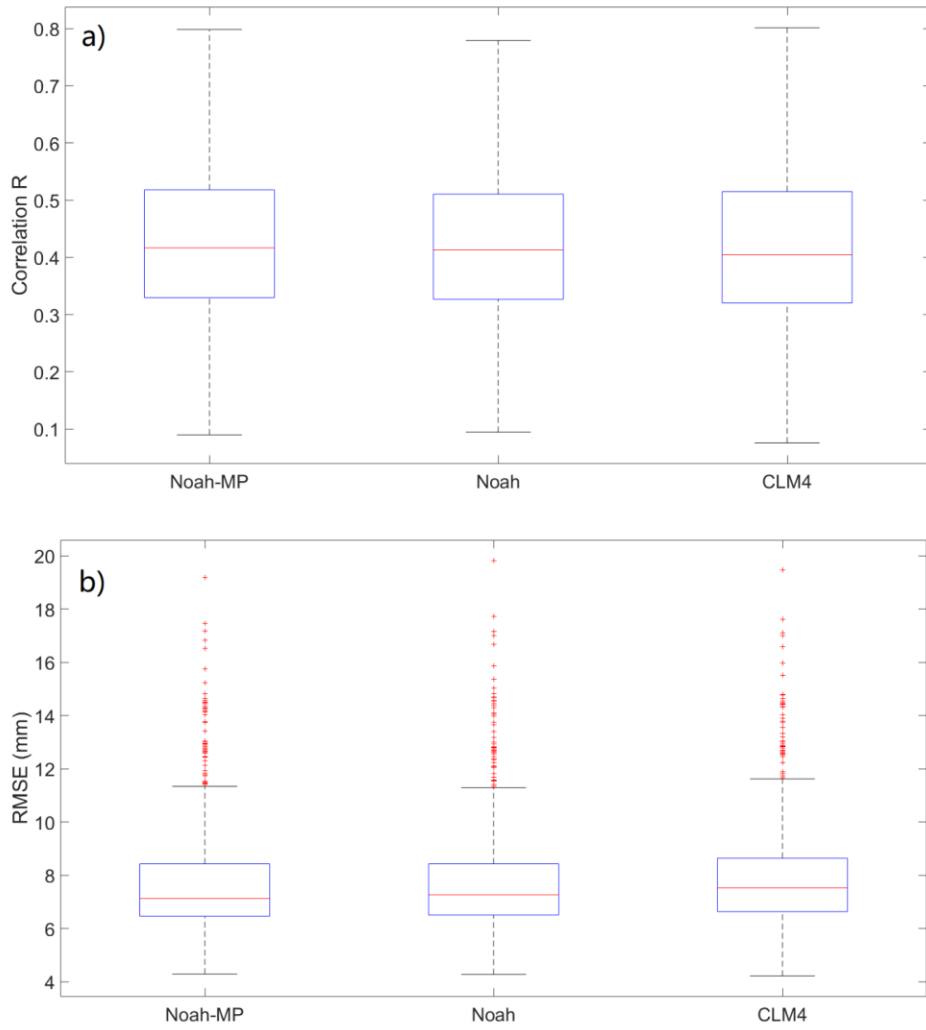


Figure 6. Boxplots of rainfall evaluation results of a) R and b) $RMSE$: minimum, maximum, 0.25, 0.50 and 0.75 percentiles, and outliers (red cross).

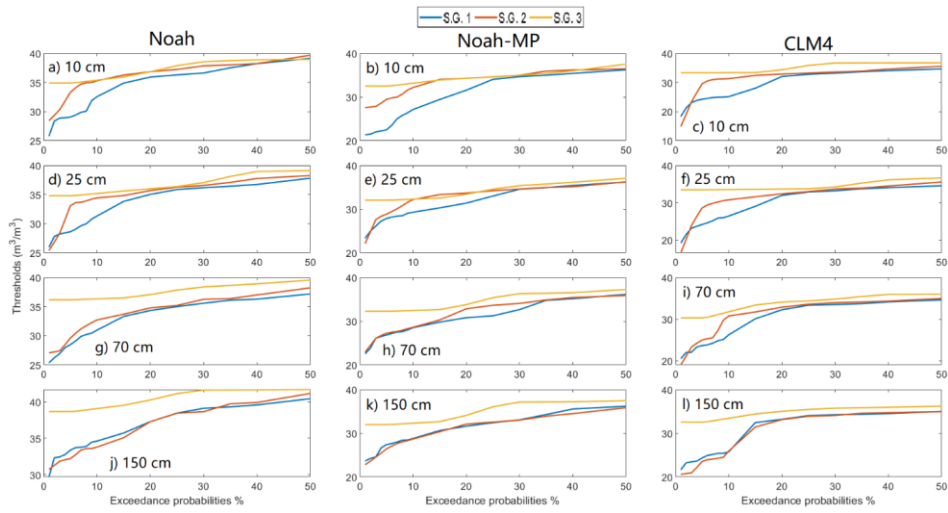


Figure 7. Threshold plots. For Noah (a, d, g, j), Noah-MP (b, e, h, k), and CLM4 (c, f, i, l) land surface schemes under three Slope angle Groups (S.G.) with S.G. 1 = 0.4-1.86°; S.G. 2 = 1.87-9.61°; S.G. 3 = 9.52-40.43°.

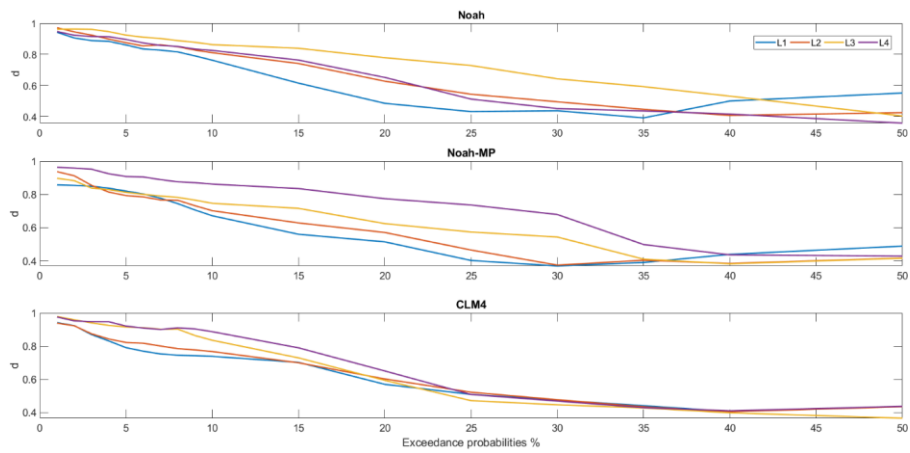


Figure 8. d-scores.

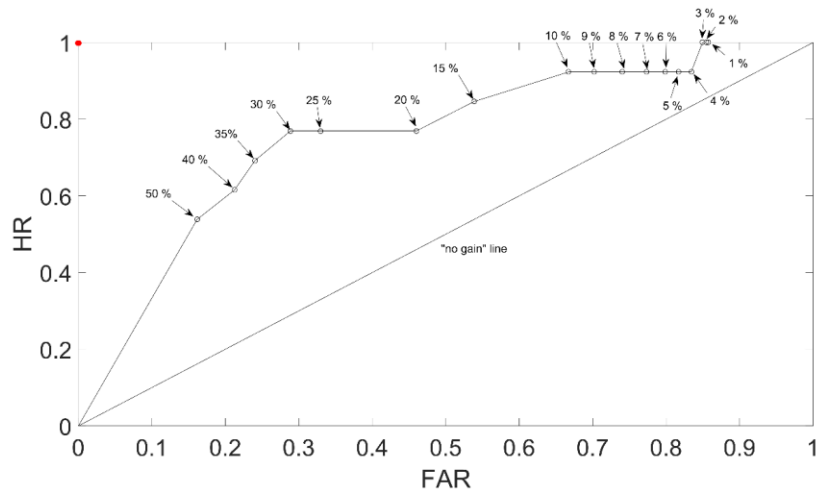


Figure 9. ROC curve for the calculated thresholds using different exceedance probability levels (for Noah-MP at the surface layer). The *no gain* line and the optimal performance point (the red point) are also presented.

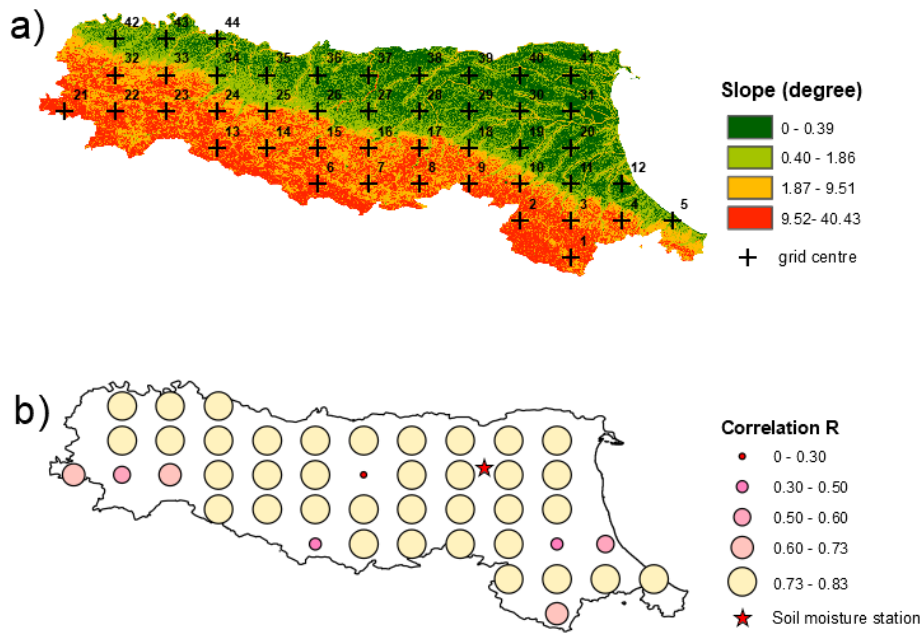


Figure 10. The cross-validation of spatially distributed WRF soil moisture against the in-situ soil moisture observation at the single point soil moisture sensor in plain area: a) grid numbers shown on the slope map, b) correlation spatial performance.

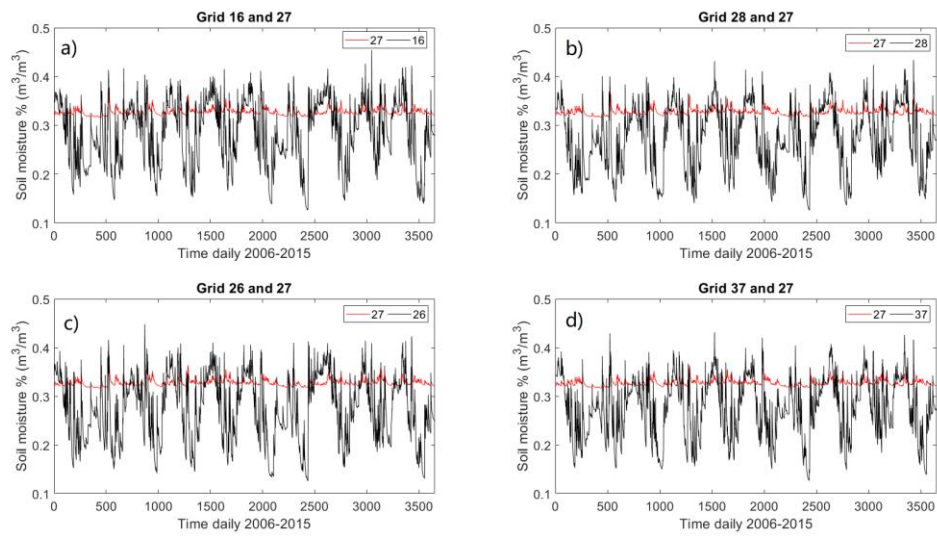


Figure 11. The soil moisture comparisons of Grid 27 with the adjacent grids (16, 28, 26, 37).